

## Comments from the Editor

There is just one single question that needs clarification. In response to Reviewer 1, you write on bullet point 11: "It means we compared two datasets both with hourly interval. The time for the sub-daily values used for model comparison were set at 10:00 am, as that usually is the time the samples were measured in the field or collected and preserved for later analysis in the lab. "

I was confused now: if you use hourly data, why do you use sub-daily data at one specific time? Can you clarify this (add also a sentence in the manuscript if appropriate).

### Response to the editor

We understand the Editor's confusion as the first paragraph of our previous response refers to the high-frequency measurements, and the second paragraph refers to the grab samples.

We now change the response into:

The time step of our model is as well an hour, which is the same as presented time series of the high-frequency measurements. The presented high frequency measurements were aggregated from 5 min (EC), 10 min (NH<sub>4</sub>), and 20 min (TP) intervals into an hourly interval. It means we compared the two datasets with both hourly interval.

We now clarified this in the text at Line 220:

*"The model provided a tool to simulate hourly concentration dynamics under the assumption that EC, NH<sub>4</sub> and TP were conservative."*

What we meant to say about the grab samples was:

The comparison between the hourly model, high-frequency and the grab sampling results was based on their concentrations at 10:00 am, as that usually was the time the grab samples were measured in the field or collected and preserved for later analysis in the lab."

We changed the text to avoid this confusion, including a previous response that we gave to reviewer 3 in the first round of our responses to the reviewers (July 30<sup>th</sup> 2020):

*Line 221: The simulated EC, NH<sub>4</sub>-N and TP were plotted together with the high frequency time series and the grab sampling data in Figure 3. Same as in Fig.2, the high frequency measurements were aggregated from 5 min (EC), 10 min (NH<sub>4</sub>), and 20 min (TP) intervals into an hourly interval. The grab sampling results were all set to be measured at 10:00 AM as that coincides with the usual grab sampling times. Additionally, a comparison between the modelled and the measured results at the annual scale was performed by using correlation analysis, aggregating the model, the high-frequency and the grab sampling results at an 4-days average.*

# Drivers of nitrogen and phosphorus dynamics in a groundwater-fed urban catchment revealed by high frequency monitoring

Liang Yu<sup>1,2</sup>, Joachim C. Rozemeijer<sup>3</sup>, Hans Peter Broers<sup>4</sup>, Boris M. van Breukelen<sup>5</sup>, Jack J. Middelburg<sup>6</sup>, Maarten Ouboter<sup>2</sup>, and Ype van der Velde<sup>1</sup>

<sup>1</sup>Faculty of Science, Vrije University Amsterdam, 1181HV, Amsterdam, the Netherlands

<sup>2</sup>Waternet Water Authority, 1096 AC, Amsterdam, the Netherlands

<sup>3</sup>Deltares, 3508 TC, Utrecht, the Netherlands

<sup>4</sup>TNO Geological Survey of the Netherlands, 3584 CB, Utrecht, the Netherlands

<sup>5</sup>Department of Water Management, Faculty of Civil Engineering and Geosciences, Delft University of Technology, Stevinweg 1, 2628 CN, Delft, the Netherlands

<sup>6</sup>Department of Earth Sciences, Faculty of Geosciences, Utrecht University, P.O. Box 80 021, 3508 TA, Utrecht, the Netherlands

*Correspondence to:* Liang Yu (xiaobaidrawing@gmail.com)

**Abstract.** Eutrophication of water bodies has been a problem causing severe degradation of water quality in cities. To gain mechanistic understanding of the temporal dynamics of nitrogen (N) and phosphorus (P) in a groundwater fed low-lying urban polder, we applied high frequency monitoring in Geuzenveld, a polder in the city of Amsterdam. The high frequency monitoring equipment was installed at the pumping station where water leaves the polder. From March 2016 to June 2017, total phosphorus (TP), ammonium (NH<sub>4</sub>), turbidity, electrical conductivity (EC), and water temperature were measured at intervals smaller than 20 minutes. This paper discussed the results at three time scales: annual scale, rain event scale, and single pumping event scale. Mixing of upwelling groundwater (main source of N and P) and runoff from precipitation on pavements and roofs was the dominant hydrological process governing the temporal pattern of the EC, while N and P fluxes from the polder were also regulated by primary production and iron transformations. In our groundwater-seepage controlled catchment, NH<sub>4</sub> appeared to be the dominant form of N with surface water concentrations in the range of 2-6 mg N/L, which stems from production in an organic-rich subsurface. The concentrations of NH<sub>4</sub> in the surface water were governed by the mixing process in autumn and winter and were reduced down to 0.1 mg N/L during the algal growing season in spring. The depletion of dissolved NH<sub>4</sub> in spring suggests uptake by primary producers, consistent with high concentrations of chlorophyll-a, O<sub>2</sub>, and suspended solids during this period. Total P and turbidity were high during winter (range 0.5-2.5 mg P/L and 200-1800 FNU, respectively) due to the release of P and reduced iron from anoxic sediment to the water column, where Fe<sup>2+</sup> was rapidly oxidised and precipitated as iron oxides which contributed to turbidity. In the other seasons, P is retained in the sediment by sorption to precipitated iron oxides. Nitrogen is exported from the polder to the receiving waters throughout the whole year, mostly in the form of NH<sub>4</sub>, but in the form of organic N in spring. P leaves the polder mainly during winter, primarily associated with Fe(OH)<sub>3</sub> colloids and as dissolved P. Based on this new understanding of the dynamics of N and P in this low lying urban catchment, we suggested management strategies that may effectively control and reduce eutrophication in urban polders and receiving downstream waters.

**Keywords:** Nitrogen and phosphorus dynamic, high frequency monitoring, benthic algae, iron chemistry, Amsterdam, groundwater seepage

## 1 Introduction

Eutrophication is one of the most notorious phenomena of water quality impairment in cities, caused by excess inputs of N and P. The identified sources of nutrients are from wastewater treatment plants, storm runoff, overflow of sewage systems, manure and fertilizer application in urban green areas and atmospheric deposition (Walsh et al., 2005; Kabenge et al., 2016; Toor et al., 2017; Yang & Toor, 2018; Putt et al., 2019). Recently, groundwater has been identified as another important source of N and P in cities situated in low-lying deltas, where dissolved NH<sub>4</sub> and PO<sub>4</sub> in groundwater seep up into urban surface water (Yu et al, 2018 & 2019). The upwelling nutrients in groundwater, originating from the organic rich delta subsurface, reaching

44 the surface water of cities and are transferred to downstream waters and eventually reach the coastal zones, where they may  
45 induce harmful algal blooms or cause hypoxia along coastlines (He and Xu, 2015; Beusen et al., 2016; Le Moal et al., 2019).  
46 Hence, it is of pivotal importance to understand N and P dynamics in the urban freshwater bodies in order to mitigate the input  
47 of nutrients into the oceans (e.g. Nyenje, et al., 2010; Toor et al., Paerl et al., 2016; 2017; Le Moal et al., 2019).  
48 Nutrients dynamics are governed by biological, chemical and physical processes and their interactions. Assimilation by  
49 primary producers is a major biological factor regulating N and P concentrations in the aquatic environment. Aquatic micro-  
50 and macro-organisms assimilate P as  $\text{PO}_4$  and N mainly in fixed forms such as nitrate ( $\text{NO}_3$ ) and ammonium ( $\text{NH}_4$ ), but for  
51 some specific organisms also in the form of  $\text{N}_2$ . In estuaries,  $\text{NH}_4$  is the preferred N-form for microbes (Middelburg and  
52 Nieuwenhuize, 2000), but the uptake rate for both  $\text{NH}_4$  and  $\text{NO}_3$  can achieve maximum rates under sustained exposure of  $\text{NH}_4$   
53 or  $\text{NO}_3$  (Bunch and Bernot, 2012). Moreover, the nitrogen species are also involved in redox transformations (Soetaert and  
54 Herman, 1995). Under anaerobic conditions,  $\text{NO}_3$  can be reduced to  $\text{NH}_4$ , in particular with high organic matter contents. It  
55 may also be denitrified to  $\text{N}_2$  and  $\text{N}_2\text{O}$  under such condition (Mulder et al., 1995), the latter is a climate-active gas. Under  
56 aerobic conditions,  $\text{NH}_4$  can be oxidized to  $\text{NO}_3$  through nitrification by nitrifying microbes, which is an  $\text{O}_2$  consuming and  
57 acid generating process. Nitrification even occurs under cold conditions (below 10 °C) (Painter, 1970; Wilczak et al., 1996;  
58 Cavaliere and Baulch, 2019).

59 The mixing of water from different flow routes is an important hydrological process that controls nutrient dynamics  
60 (Rozemeijer and Broers, 2007; Rozemeijer et al., 2010a; Van der Grift et al., 2014; Yu et al., 2019). As nutrient concentrations  
61 and speciation differ among different flow routes (Wriedt et al., 2007; Rozemeijer et al., 2010a; Yu et al., 2019; Yang and  
62 Toor, 2019), the mixing process results in dilution or enrichment of nutrients in surface water bodies during precipitation  
63 events (Wang et al., 2016).

64 Retention is another factor that determines nutrient concentrations and transport (McGlathery et al., 2001; Zhu et al., 2004;  
65 Henry and Fisher, 2003), especially for phosphorus most of which is retained in inland water bodies sediment (Audet et al.,  
66 2019). The retained P are either being permanently buried in the sediment or temporarily stored and acting later on as internal  
67 nutrient source (Kleeberg et al., 2007; Filippelli, 2008; Zhang et al., 2018). Multiple researchers have highlighted the influence  
68 of iron chemistry on the dynamics of P in pH neutral environments (Chen et al., 2018; Van der Grift et al., 2018). This is  
69 especially relevant when iron-rich groundwater interacts with surface water (Griffioen, 2006; Rozemeijer et al., 2010a; Van  
70 der Grift, 2014; Yu et al., 2019), in which P is immobilized by the formation of iron(oxy)hydroxides during groundwater  
71 aeration. However, changes in chemistry or temperature may lead to the release of P and reduced iron. For instance, under  
72 anaerobic conditions, Fe and P can be mobilized by sulfate reduction, but this can be counteracted by the presence of  $\text{NO}_3$  as  
73 electron acceptor (Smolders et al., 2006).

74 Most studies of eutrophication are based on discrete sampling events which can give a general pattern of nutrient dynamics,  
75 but can easily miss important nutrient transport and processing phenomena (Rozemeijer et al., 2010; Rode et al., 2016; Toor  
76 et al., 2017). The countermeasures to control eutrophication have been hampered because of limited knowledge of N and P  
77 dynamics, for instance their response to changing weather conditions and land use (van Geer et al., 2016). In the past few years,  
78 the development of new sensors and sampling technologies allow us to obtain data with substantially shorter intervals. In this  
79 paper, the high frequency monitoring technology is referred to as an automatic monitoring program with sampling and  
80 analyzing frequencies that are sufficient for obtaining detailed water quality variation information. High frequency technology  
81 has proved to be a way to understand nutrient dynamics (Rode et al., 2016; Van Geer et al., 2016; Bieroza et al., 2018). Due  
82 to the abundant information offered by this technology, combined methodologies have been developed to quantitatively  
83 understand the in stream hydrochemistry of nutrients (Miller et al., 2016, Van der Grift et al., 2016, Duncan et al., 2017).

84 In our previous study on the water quality of Amsterdam (Yu et al, 2019), the transport routes of N and P from groundwater  
85 to surface water through seepage and drains were identified. In addition, spatial and temporal concentration patterns from  
86 discrete sampling campaigns showed a clear dilution pattern of other water quality parameters such as EC. However, the

87 temporal patterns of N and P were still poorly understood, probably due to their reactive nature and more complex  
 88 biogeochemistry. In order to obtain insight into the controlling mechanisms of N and P transport and fate in urban delta  
 89 catchments affected by groundwater, we performed a year-round high-resolution N and P concentration monitoring campaign.  
 90 A deep understanding of the water quality dynamic drivers would be a great asset for controlling eutrophication and improving  
 91 aquatic ecological status (Fletcher et al., 2015; Díaz et al., 2016; Eggimann et al., 2017; Nizzoli et al., 2020). We conducted a  
 92 one-year high frequency monitoring campaign in 2016-2017. Measured parameters were EC, NH<sub>4</sub>, TP, turbidity and water  
 93 temperature. The temporal patterns of these parameters were studied at three time scales: the annual scale, rain event scale,  
 94 and pumping event scale.

## 95 2 Methods

### 96 2.1 Study site

97 The Geuzenveld study site is part of an urban lowland polder catchment, which is characterized by groundwater seepage that  
 98 constantly determines the surface water quality, being the main source of solutes in the water system. The groundwater seepage  
 99 is a continuous source of slightly brackish, anoxic, and iron and nutrient rich water. Yu et al. (2019) presented the results of a  
 100 10 year monitoring program describing the main processes determining the water quality in the catchment, which is dominated  
 101 by mixing of runoff water and seepage water. A high-frequency monitoring campaign was set-up to further unravel the  
 102 temporal patterns of the nutrient N and P, of which N is typically present in the form of NH<sub>4</sub> from groundwater.

103 Geuzenveld is a newly built urban polder on the west of the city of Amsterdam (Fig.1). Since the 1990s, when it was converted  
 104 from agricultural to urban land, it has developed into a highly paved area. Similar to other new neighborhoods, Geuzenveld is  
 105 equipped with a separated drainage system. A rain harvesting system was installed on all the buildings and houses in the polder,  
 106 leading rain water from the roof and the street directly to the ditches, which results in fast and large amounts of runoff during  
 107 storm events. Geuzenveld is a groundwater fed catchment due to the constantly higher groundwater head (-2.5 ~ -3 m NAP,  
 108 NAP: Normalized Amsterdam Peil) in the main aquifer relative to the surface water level in the polder ditches (~ -4.25 m NAP)  
 109 (Fig.2). To keep the foundations of the building dry, there is a groundwater drainage system placed under an artificial sandy  
 110 layer, right on top of a natural clay layer. The drain elevations range from -4.84 to -4.61 m NAP, which is below the phreatic  
 111 groundwater level throughout the year, making sure that groundwater seepage either discharges through the drains or the  
 112 ditches.

113 The water system of Geuzenveld is connected to the secondary water channel to its east, then connected to the adjacent primary  
 114 channel, called boezem, the Boezem Haarlemmerweg. The boezem water level is -2.10 m NAP. It is much higher than the  
 115 target surface water level of Geuzenveld, -4.25 m NAP. The surface water level in polder Geuzenveld is controlled by a pump  
 116 station, which is the main outlet of this polder, situated in the northeastern corner.

117 There are two pumps (Pump 1 and Pump 2) in the pumping station, and they have different start and end pumping threshold  
 118 points (Table 1).

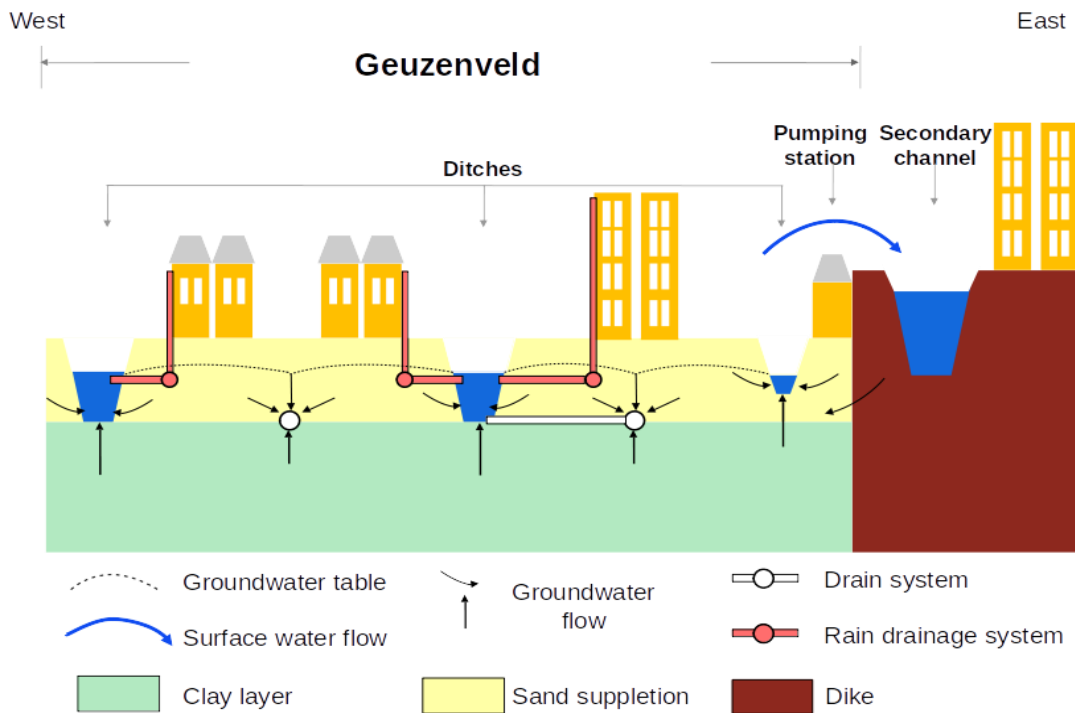
119 **Table 1 Pumping scheme of polder Geuzenveld**

Time	Settings	Pump 1	Pump 2
05:00:00-19:00:00	Start point (m NAP)	-4.20	-4.16
	End point (m NAP)	-4.26	-4.24
19:00:00-05:00:00	Start point (m NAP)	-4.23	-4.18
	End point (m NAP)	-4.31	-4.29

120

121

122 The two pumps are activated when the surface water level exceeds the triggering level which are furthermore separated as day  
 123 and night triggering levels (Table 1). The capacity of each pump is 3.6 m<sup>3</sup> per minute. Most of the time, only one of the two  
 124 pumps works and the surface water level is maintained between -4.31 m NAP and -4.23 m NAP, which are the night inactive  
 125 and active pumping levels respectively. Normally, the surface water level drops immediately when the pump(s) start(s)  
 126 working. Once the pump(s) stop(s), the surface water level will steadily rise due to the continuous inflow of groundwater  
 127 seepage. During rainfall events, the surface water level rises faster (Fig.2A).



128



129

130 **Figure 1** Location of polder Geuzenveld (source: © Google Maps ) and its landscape cross section and rain water and  
 131 groundwater drainage system

## 132 2.2 Monitoring network setup

### 133 2.2.1 High frequency monitoring

134 A high frequency monitoring network was built on a temporary floating platform in front of the pumping station. The water  
135 flowed around and underneath this platform to the pumping station when the pumps started working. One year time series of  
136  $\text{NH}_4\text{-N}$  ( $\text{mg L}^{-1}$ ), TP (and ortho-P) ( $\text{mg L}^{-1}$ ), turbidity (Formazin Nephelometric Unit, FNU), electrical conductivity (EC,  $\mu\text{S/cm}$ )  
137 and water temperature ( $^{\circ}\text{C}$ ) were collected by the following equipment: a Sigmatax sampler combined with a Phosphax sigma  
138 auto analyser for total phosphorus (TP), Amtax for  $\text{NH}_4\text{-N}$  combined with a Filtrax automatic sampler, a Solitax-tline sc for  
139 turbidity (manufactured by: Hach Lange GmbH Düsseldorf, Germany), and CTD-Diver for electrical conductivity (EC) and  
140 water temperature (manufactured by: Van Essen Instruments, Delft, The Netherlands). The monitoring frequencies were set  
141 to 20 mins, 10 mins, 5 mins, 5 mins and 5 mins interval for TP,  $\text{NH}_4\text{-N}$ , turbidity, EC and water temperature, respectively.

142 The Phosphax sigma is an analogue analyser for the high precision determination of total phosphorus concentration in  
143 accordance with EN 1189 Phosphormolybdenum Blue method. Samples are automatically taken through a Sigmatax sampling  
144 probe and include suspended solids. Subsequently, the sample is ultrasonic homogenized before delivery to the Phosphax  
145 sigma. It is digested by the sulphuric acid-persulphate method (APHA/WWA-WPCF, 1989), and analysed with a LED  
146 photometer (at 880 nm) (Hach, user manual of Phosphax sigma, 2016).

147 Samples for  $\text{NH}_4$  are prepared by a filtration system, Filtrax. It continuously extracts samples through two ultra-filtration  
148 membranes ( $0.15\ \mu\text{m}$ ) plates. Particles get dispersed by a continuous aeration system near the surface of the membranes (The  
149 aeration caused severe build-up iron precipitants on the plates). The samples are then delivered to Amtax sc for analysis. The  
150 ammonium in the sample is first converted to gaseous ammonia. Only the  $\text{NH}_3$  gas passes through the gas-permeable membrane  
151 of the electrode and is detected. This method guarantees a wide measuring range and is less sensitive to other compounds  
152 compared to methods that make use of an ion-selective electrode (ISE). The Amtax sc in our study was calibrated automatically  
153 at 22:00 every 24 hours before September 2016, every 48 hours thereafter. Maintenance work was conducted weekly as the  
154 tubes were easily blocked by iron precipitates (Hach, user manual of Amtax sc, 2013).

155 The Solitax-tline sc sensor is a turbidity sensor with dual-beam optics and added backscatter. The measuring principle is based  
156 on a combined infrared absorption scattered light technique that measures the lowest turbidity values in accordance with DIN  
157 EN 27027 just as precisely and continuously as high sludge contents. Using this method, the light scattered sideways by the  
158 turbidity particles is measured over an angle of  $90^{\circ}$  (Hach, User manual of Solitax sc, 2009).

159 The monitoring period of  $\text{NH}_4$  and turbidity is from 2016-05-10 to 2017-06-16. Time series of phosphorus were obtained from  
160 2016-05-23 to 2017-06-16. Electrical conductivity and temperature data are from 2016-06-10 to 2017-06-15. The  $\text{NO}_3$  analyser,  
161 Nitratax, time series consistently showed an artificial drift and proved to be unreliable in our field setting, possibly due to  
162 biofilm accumulation in combination with iron oxides precipitation (see discussion). All the equipment outputs were integrated  
163 into one wireless station. The monitoring station was shut down several times by lightning, so an electricity restart program  
164 was also applied in this network. It worked for all equipment except for the Phosphax, which had to be restarted manually after  
165 a black out.

166 Precipitation (hourly) and Evapotranspiration (daily) data were downloaded from the Schiphol KNMI station which is about  
167 2 km away from Geuzenveld. Hourly pumping activity and surface water level data were obtained from Waternet, the water  
168 authority of Amsterdam.

### 169 2.2.2 Low frequency monitoring

170 Since 2006, Waternet has monitored the water quality with a frequency of 12 times per year by sampling at the pumping station  
171 of Geuzenveld. Between 2016 and 2017, the sampling frequency was increased to twice per month. We selected the following  
172 parameters from the routine monitoring campaign: (1) EC,  $\text{NH}_4\text{-N}$  and TP to fill in the gaps in the continuous time series, and

173 to verify and monitor the potential drift and offset of the high frequency data and (2) pH, O<sub>2</sub>, HCO<sub>3</sub>, NO<sub>3</sub>, TN, Kjeldahl-N,  
 174 suspended solids (detail of methods are described by Yu et al, 2019), chlorophyll-a, and transparency for further understanding  
 175 the biogeochemical processes. Organic-N was estimated by subtracting NH<sub>4</sub>-N from Kjeldahl-N.  
 176 Bi-weekly total iron in the water column was analysed separately using ICP-AES (inductively coupled plasma-atomic emission  
 177 spectrometry). Total Fe was analysed from samples to which HgCl<sub>2</sub> was added for preservation and that were stored in a dark  
 178 and cool environment. To release all Fe that may have sorbed or precipitated during storage, we added 1 or 0.5 ml HCl in the  
 179 water samples to dissolve eventual flocks. Then the samples were homogenized in an ultrasonic bath for 24h, mixed again to  
 180 break down all the flocks. For extraction of all the Fe, we transferred 10 mL of the homogenized sample into a Teflon bottle,  
 181 added 3.2 mL HCl : HNO<sub>3</sub> 3:1 , and stored in a stove at 90 °C for 24 hours. The final solutions were analysed by ICP-AES.  
 182 Blanks were included and treated identical to samples.

### 183 2.3 Data processing and analysis

184 A correlation analysis between the high frequency and discrete monitoring data was applied to illustrate the reliability of the  
 185 high frequency time series. Furthermore, the time series data were analysed at 3 time scales: annual scale, rainfall events  
 186 (several days) and single pumping events (several hours). The relationships among the monitored parameters was explored by  
 187 testing their correlations at each time scale. At the annual scale, a correlation analysis was applied to the complete time period  
 188 and the wet and dry periods (definition in section 3.1.1). To discern the hydrological and chemical/biological attributes to the  
 189 observed dynamics, a linear mixing model was introduced at the annual scale, assuming precipitation and groundwater seepage  
 190 are the only water inputs, pumping and evapotranspiration are the only outputs, and pumping activity is the only way solutes  
 191 leave the water system. In this model, we assumed a constant seepage rate. Accordingly, surface water level was calculated  
 192 from:

$$194 \frac{dV}{dt} = (P(t) + S - E(t)) * A_{polder} - Pump(t) \quad (1)$$

$$195 L(t) = V(t)/A_{ditch} \quad (2)$$

196  
 197  $V$  is total water volume in the ditches,  $P$  is precipitation,  $S$  is a constant seepage,  $E$  is potential evapotranspiration,  $A_{polder}$  is  
 198 area of the polder,  $Pump(t)$  is water volume being pumped out with maximum capacity 216 m<sup>3</sup> h<sup>-1</sup>,  $A_{ditch}$  the area of the ditches  
 199 in the polder.  $L$  is surface water level in the ditches. Water level  $L$  determines the activation of pumping activity. Once  $L(t)$   
 200 exceeds the upper ranges of water level (start point, section 2.1), the pumps will start to pump until  $L$  goes below the stopping  
 201 end (section 2.1) in the pumping scheme. Given the year-round seepage conditions throughout the polder, combined with an  
 202 artificially drained subsurface, we assumed that the potential evapotranspiration was close to the actual evapotranspiration  
 203 as no water shortages occur in our situation. In this study, we used the difference between groundwater head in the first  
 204 aquifer and the surface water level (Figure 2A) to estimate a range of the seepage. The actual number of 2 mm per day was  
 205 chosen based on the behavior of the mixing model and calibrated using the measured surface water levels (Figure S1).

206 A complete mixing of solutes was assumed in the model, which means that seepage, ditch water and precipitation mix  
 207 instantaneously when they enter the surface water. A delay from precipitation to run-off/drainage and to ditches was not  
 208 specifically considered.

$$210 \frac{d(VC)}{dt} = S * A_{polder} * C_{gw} + P(t) * A_{polder} * C_P - Pump(t) * C(t) \quad (3)$$

211



212  $V$  is the ditch water volume given by equation (1),  $C(t)$  is solute concentration at time  $t$ ,  $C_{gw}$  is the average groundwater  
213 concentration,  $C_p$  is the average concentration in runoff.

214 In our study area, the EC is a useful water quality parameter for describing the mixing processes between groundwater and  
215 runoff water, as the EC represents the end members of the mixing: groundwater with an high EC (1750  $\mu\text{S}/\text{cm}$ ) and runoff  
216 water (100  $\mu\text{S}/\text{cm}$ ) with a low EC (see also Yu et al., 2019). Moreover, we assume that EC behaving as a conservative tracer  
217 as the EC is highly correlated with the Cl concentration ( $R^2 = 0.71$ ,  $p$ -value  $< 0.05$ ) and the temporal patterns of EC and Cl are  
218 very similar (see supplement Figure S2). In the model, seepage rate was adapted to get the best fit between the modeled and  
219 the measured EC. The calibrated seepage rate was 2.0  $\text{mm d}^{-1}$ . Compared to EC, nutrients are highly reactive solutes and thus  
220 can vary a lot along their flow routes due to biogeochemical processes. The model provided a tool to simulate hourly  
221 concentration dynamics under the assumption that EC,  $\text{NH}_4$  and TP were conservative. ~~The simulated concentrations of EC,~~  
222  ~~$\text{NH}_4$ -N and TP were plotted together with the high frequency measured time series. A comparison between the modeled and~~  
223 ~~the measured results was performed by using correlation analysis. The simulated EC,  $\text{NH}_4$ -N and TP were plotted together~~  
224 with the high frequency time series and the grab sampling data in Figure 3. Same as in Fig.2, the high frequency measurements  
225 were aggregated from 5 min (EC), 10 min ( $\text{NH}_4$ ), and 20 min (TP) intervals into an hourly interval. The grab sampling results  
226 were all set to be measured at 10:00 AM as that coincides with the usual grab sampling times. Additionally, a comparison  
227 between the modeled and the measured results at the annual scale was performed by using correlation analysis, aggregating  
228 the model, the high-frequency and the grab sampling results at an 4-days average.

229 The average concentration of EC in groundwater was set equal to the average of the sampling survey, which was 1750  $\mu\text{S}/\text{cm}$   
230 (including both deep and shallow groundwater, Yu et al., 2019). For the  $\text{NH}_4$  and TP concentration data, we chose the  
231 measurement from a drain sampling point (Drain 3, Yu et al., 2019) in the middle of the polder as the non-disturbed  
232 groundwater collected by the drains in this area of the polder. They were 8.1  $\text{mg N L}^{-1}$  and 1.6  $\text{mg L}^{-1}$  respectively. The starting  
233 (01-06-2015) concentrations were 1200  $\mu\text{S}/\text{cm}$ , 4  $\text{mg L}^{-1}$ , and 2  $\text{mg L}^{-1}$  for EC,  $\text{NH}_4$ , and TP respectively. The model was not  
234 sensitive to the selected end-member values.

235 The time series data were further analysed at shorter scales: rain event scale and pumping event scale. Four rain events were  
236 selected according to the dilution extent of EC, defined as an EC value reduced by over 35%, they were: 10-06-2016 ~ 15-07-  
237 2016, 15-08-2016 ~ 26-09-2016, 10-11-2016 ~ 05-01-2017, and 20-02-2017 ~ 10-04-2017. These four events covered both  
238 EC dilution during rainfall and the recovery afterwards in different seasons. We selected 4 representative pumping events to  
239 present the response of EC,  $\text{NH}_4$ , TP, and turbidity to the pumping activities. Those events were in 15-07-2016 ~ 17-07-2016,  
240 27-10-2016 ~ 29-10-2016, 20-12-2016 ~ 22-12-2016, and 05-05-2017 ~ 07-05-2017. Correlation analysis was as well applied  
241 to each event at the corresponding two time scales, averaging over whole days for precipitation events and over hours for  
242 pumping events. Data processing and analyzing were performed using Rstudio (R version 4.0.2) and time series package “xts”.

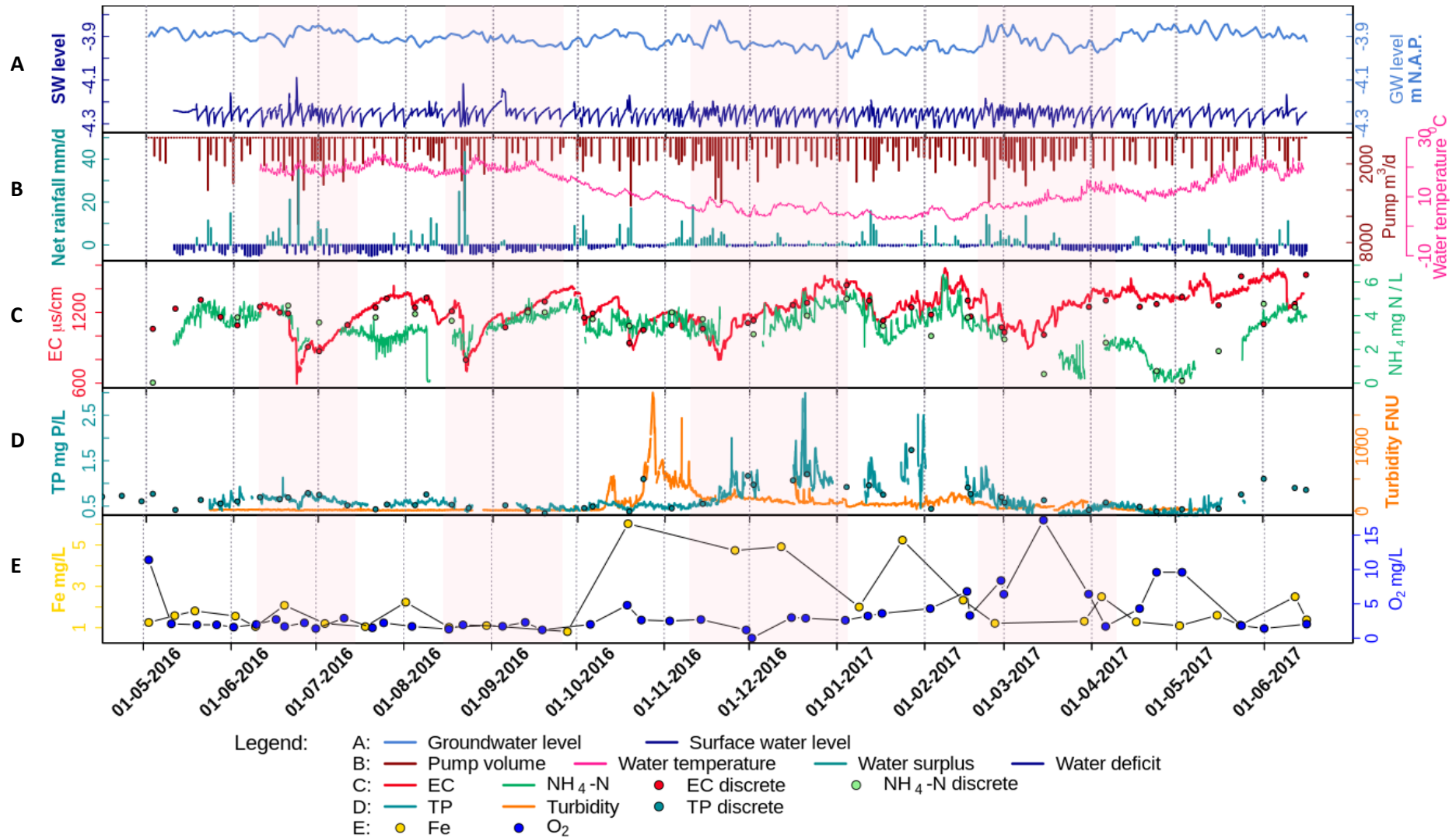
## 243 3. Results

### 244 3.1 Annual pattern of meteorological, hydrological, and water quality time series

#### 245 3.1.1 Meteorological and hydrological conditions in polder Geuzenveld

246 To explain the time series (Fig. 2), we distinguish between dry/wet periods and dry/wet seasons. The wet and dry periods (days  
247 to weeks) are represented by a water surplus (light blue color in Fig.2B, daily evapotranspiration  $<$  daily precipitation) or a  
248 water deficiency (dark blue in Fig.2B, daily evapotranspiration  $>$  daily precipitation). We defined the wet and dry seasons  
249 based on water surplus and deficit. The average net rainfall (the water surplus/deficit in Figure 2) is 1.4  $\text{mm}/\text{d}$  for the period  
250 of 01-10-2016~15-03-2017, and -0.8  $\text{mm}/\text{d}$  for the rest. Subsequently, we statistically analysed the difference between these  
251 two periods for multiple parameters. Table 2 shows the mean of each parameter for the wet and dry seasons and their  
252 significance test results. The wet and dry seasons means are significantly different for all parameters, but the EC.





253  
 254 **Figure 2** Time series of (A) surface water level (SW level) and groundwater level (m NAP), (B) net rainfall (daily water surplus (+) (lightblue) and deficit (-) (darkblue), mm d<sup>-1</sup>)  
 255 and daily pumping volume (Pump m<sup>3</sup> d<sup>-1</sup>), (C) hourly time series of EC (μS/cm) and NH<sub>4</sub>-N (mg N L<sup>-1</sup>), and (D) hourly TP, turbidity, (E) discrete samples of Fe (total iron in  
 256 water column) and O<sub>2</sub> concentrations (mg L<sup>-1</sup>). The dots in (C) and (D) are the corresponding discrete sampling data, which are plotted to show their close match to the  
 257 continuous time series data, as well as to fill in the gaps. All data were monitored at the pump station. The transparent pink blocks are the selected rain events for further  
 258 analysis in section 3.3. See Table S1-S3 for the correlation tests performed on the dataset.

**Table 2 The mean of each parameter, and the significance for the wet and dry seasons**

	Net rainfall* mm/d	Pump volume* m <sup>3</sup> /d	Water temperature* °C	EC µs/cm	NH <sub>4</sub> * mg N/L	TP * mg P/L	Turbidity* FNU	Fe* mg/L	O <sub>2</sub> * mg/L
Wet	1.4	1050	6.7	1212	3.7	0.8	197	3.4	4.3
dry	-0.8	712	17	1252	3.0	0.5	15	1.5	3.3

260 \*  $p < 0.05$ <sup>1</sup>

261

262 Over the whole monitoring period, the water temperature ranged between 2 to 26 °C. From June to mid-September 2016, the  
263 temperature remained above 18 °C, then declined to become lower than 10 °C at the end of October. The following four months  
264 (November to February) were the coldest. Especially in January and February 2017, during which the water temperature  
265 dropped to below 3 °C. By the end of February temperatures started to rise again to reach 10 °C by the end of March 2017.

266 The surface water level in Geuzenveld has been maintained between -4.31 and -4.1 m NAP, strictly regulated by pumping  
267 (Fig.2A). After the pumps stopped, the surface water level recovered faster during the wet season (between October 2016 and  
268 March 2017) than during the dry season. Similarly, the shallow groundwater level positively corresponded to the precipitation  
269 and negatively to the daily accumulative pumping volume. The phreatic groundwater level in Fig.2A (light blue) was from  
270 one of the piezometers, which lies right outside of the polder (Figure 1, 52°22'46.0"N 4°47'15.6"E). In contrast to the constant  
271 surface water levels (Fig.2A, dark blue), the shallow groundwater had relatively low levels in the wet season compared to the  
272 dry season. This is related to the water level regulation of the boezem Haarlemmerweg with higher levels in summer than in  
273 winter (<https://www.rijnland.net/actueel/water-en-weer/waterpeil>). Phreatic water levels were consistently 20-40 cm higher  
274 than the surface water level in the polder, which confirms the continuous groundwater seepage into the surface water system.

### 275 3.1.2 Annual water quality patterns

276 The Pearson's coefficients of determination ( $R^2$ ) between the high frequency data and the routine discrete sampling data from  
277 the water authority are 0.88 for EC ( $p$ -value < 0.05), 0.92 for NH<sub>4</sub> ( $p$ -value < 0.05), and 0.97 for TP ( $p$ -value < 0.05). The  
278 scatter plots between the high and low frequency measurements are shown in Figure S7.

279 During a rainfall event, rain and runoff from pavements and roofs, which were collected by a separate drainage system, directly  
280 fed the surface water (Fig.1). Distinct rainfall events cause a strong dilution pattern of both EC and NH<sub>4</sub> (in Fig.2C). The EC  
281 ranged from 600 to 1500 µS/cm. In general, during rainfall events, the EC declined because of dilution, while, after the events,  
282 EC gradually rose back up to around 1500 µS/cm. The duration of this process, i.e. *recovery time*, was longer in the wet season  
283 than in the dry season. A similar pattern of dilution and recovery is also visible for NH<sub>4</sub>, especially for the period August 2016  
284 – March 2017, where NH<sub>4</sub> shows a very similar response as EC (Table S2, wet season,  $R^2 = 0.73$ ), although with somewhat  
285 larger day to day fluctuations. However, a contrasting pattern without NH<sub>4</sub> recovery occurred twice: from the middle of June  
286 to the end of August 2016 and from the middle of March to the middle of May 2017. During these periods, concentrations of  
287 NH<sub>4</sub> were considerably lower and deviated from the slope of the EC pattern. NH<sub>4</sub> decreased from around 4 mg L<sup>-1</sup> to around  
288 2 mg L<sup>-1</sup> between the middle of June to the end of August 2016, but the continuous NH<sub>4</sub> measurements are not supported by  
289 the discrete samples which follow the EC pattern more closely. During the second period from March to the middle of May  
290 the deviation from the recovery pattern is more pronounced, and NH<sub>4</sub> concentrations dropped to almost 0 mg L<sup>-1</sup> and started  
291 recovering from the beginning of May. This pattern is fully supported by the available discrete samples. During the same  
292 period in 2016 the high-frequency monitoring had not yet started, a single NH<sub>4</sub> discrete measurement is available for the 2<sup>nd</sup>  
293 of May, that seems to reveal a similar pattern in the spring of 2016.

<sup>1</sup> Wilcoxon rank-sum test. The tests were performed in Rstudio (version 3.6.1), wilcox.test() in package "stats".

294 Both TP and turbidity showed contrasting patterns during the wet and dry seasons (Fig. 2D). Turbidity stayed below 60 FNU  
295 during the dry season until October and rapidly increased after a first rain event to 500 FNU (more details refer to Figure S3  
296 in supplementary information). A drop to about 200 FNU occurred right after this first peak, which seemed to correspond to  
297 excessive precipitation and a large pumping volume (Fig.2B). Soon after, turbidity went up again and peaked at 1800 FNU.  
298 Turbidity leveled off towards values around 200 FNU for the rest of the wet season and dropped below 60 FNU from April  
299 2017 onwards.

300 TP concentrations were significantly higher during the period between 15-11-2016 and 01-03-2017 than the rest of the time  
301 ( $p$ -value  $< 0.001$ , Figure S5), during which TP fluctuated around  $0.5 \text{ mg L}^{-1}$ , but always below  $1 \text{ mg L}^{-1}$ . During the wet season  
302 with the low temperatures (Table S2,  $R^2 = -0.68$ ), TP almost constantly stayed above  $1 \text{ mg L}^{-1}$  and even reached values of  
303 about  $3 \text{ mg L}^{-1}$  in December. Although there were large gaps in the TP time series during this period, the high TP concentrations  
304 appear to have been diluted by rain events, for example the event at around January 10<sup>th</sup>, 2017. Most discrete samples  
305 measurements of TP matched well with values from the high frequency time series (Fig.2D, Table S1,  $R^2 = 0.88$ ).

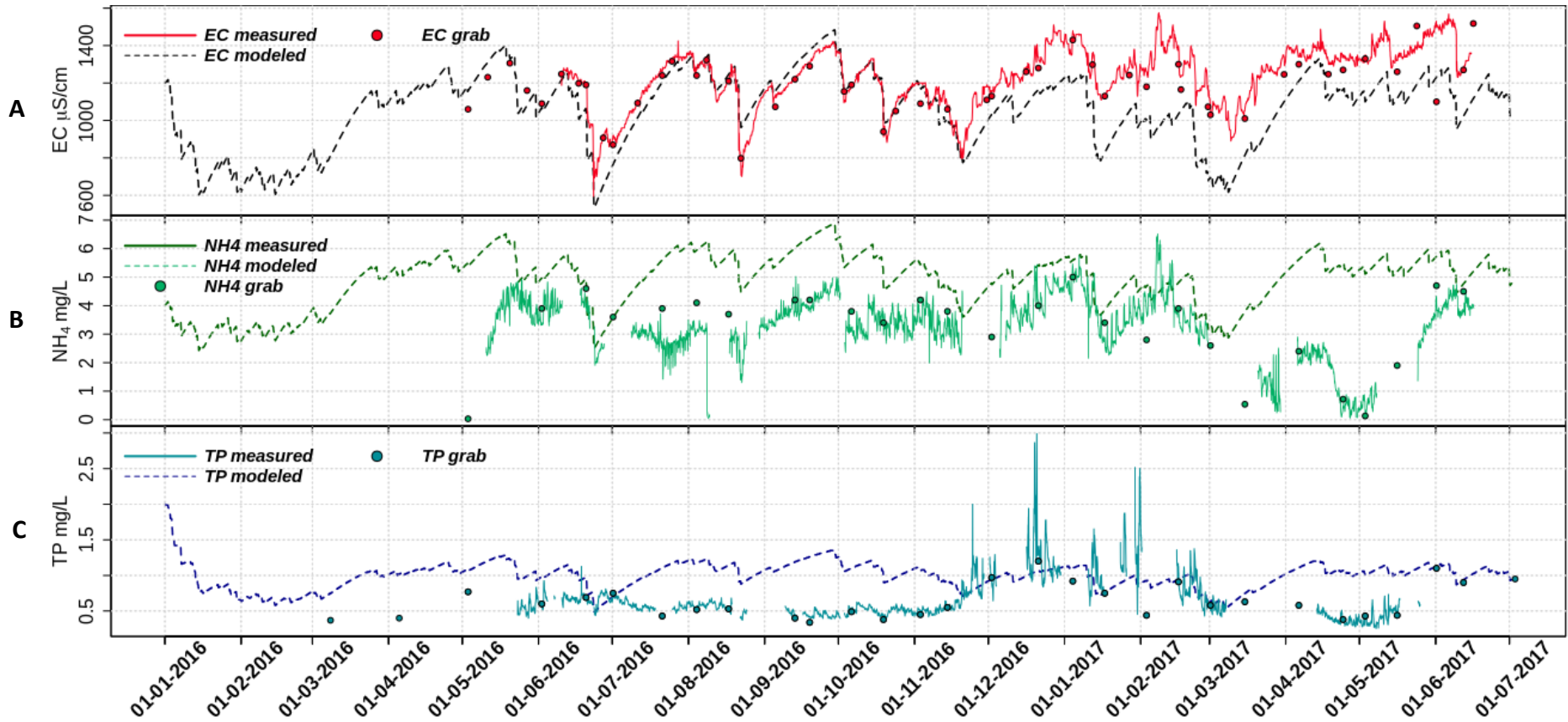
306 Total-Fe concentrations were most of time lower than  $2 \text{ mg L}^{-1}$  (Fig. 2E), but for the wet season concentrations were higher  
307 and reached up to about  $6 \text{ mg L}^{-1}$ . The initiation of Fe increases at the beginning of the wet season coincided with that of  
308 turbidity (Fig.2D and Table S2,  $R^2 = 0.72$ ). Upon the increasing temperature in March 2017, total Fe concentrations dropped  
309 back to below  $2 \text{ mg L}^{-1}$  (a negative correlation between temperature and Fe is shown in Table S1). Dissolved  $\text{O}_2$  concentrations  
310 were generally low in the water column; i.e. usually below  $5 \text{ mg L}^{-1}$ . Concentrations of over  $3 \text{ mg L}^{-1}$  were only found in  
311 March, April and May.

### 312 **3.2 Model of water quality time series based on water balance**

313 A simple fixed-end-member mixing model was used to reconstruct the conservative mixing of EC,  $\text{NH}_4$ , and TP. The simulated  
314 and the measured EC,  $\text{NH}_4$ , and TP are plotted in Figure 3. The correlations between the modeled and measured results are  
315 shown in the supplementary information (Table S4-S6). Potential processes that might deprive or enrich nutrients relative to  
316 the conservative mixing process along the flow routes were inferred from the discrepancies between the modeled and the  
317 measured data. Figure 3(A) and Table S5 show that the predicted and observed EC dynamics agree reasonably well from May  
318 to November 20<sup>th</sup>, 2016 ( $R^2 = 0.91$ ). After that, the conservative mixing approach underestimated the EC but the main dynamics  
319 and the amplitudes were still reproduced (Table S6,  $R^2 = 0.82$ ); as groundwater is the only contributor to the high EC due to  
320 the seepage of quite mineralized, slightly brackish water, the model must underestimate the seepage flux from November 20<sup>th</sup>,  
321 2016 on. Overall, the observed dynamics of EC are consistent with mixing of high EC seepage water with low EC runoff water  
322 (coefficient of determination between the modeled and measured EC is 0.65 over the complete period, Table S4).

323 The dynamics of measured  $\text{NH}_4$  concentrations show close resemblance to the model results, especially during the wet season  
324 (01-10-2016~15-03-2017). Clearly,  $\text{NH}_4$  is diluted during the rain events and a gradual increase of  $\text{NH}_4$  starts after each rain  
325 event during the wet season showing slopes that resemble the model reconstruction. Over the whole period, measured  $\text{NH}_4$   
326 concentrations were overestimated by the model, indicating that some  $\text{NH}_4$  is probably lost due to non-conservative processes.  
327 This is especially true for the spring season of 2017, where  $\text{NH}_4$  concentrations must be controlled by additional processes.  
328 Concentrations of TP are generally far below the conservative model reconstruction, except between the end of November and  
329 the beginning of March. During this particular period the minimum measured TP concentrations are captured nicely by the  
330 conservative model, but the distinct peaks up to  $3 \text{ mg L}^{-1}$  are not .

331



332  
 333  
 334  
 335  
 336

Figure 3 Plots of fixed-end-member mixing model predicted (A) EC, (B) NH<sub>4</sub> and (C) TP with their measured time series data and the discrete sampling results. See Table S4-S6 for the correlation tests performed on the dataset.

### 337 3.3 Water quality responses to single events analysis

338 To elucidate the response pattern of water quality to precipitation and pumping activity, we selected four major events (Fig.2  
339 (4 pink shades) and Figure 4) and four pumping events (Figure 5). The former events were chosen according to their clear  
340 dilution pattern of EC (Fig.4), while the latter were pumping events without occurrence of rainfall (Fig.5). All seasons were  
341 covered, including some of the wet and dry periods.

#### 342 3.3.1 Rainfall events

343 EC and NH<sub>4</sub> showed clear dilution and recovery patterns during all events, while the pattern was not clear for TP and turbidity  
344 (Fig.4). The extent of dilution of EC appears to depend on the precipitation intensity. Rainfall during the recovery period  
345 determined how long it took to recover back to the highest level. The short but intensive rainfall during dry season events 1  
346 and 2 reduced EC rapidly from around 1300 to around 700  $\mu\text{S}/\text{cm}$ , while the recovery took about 1 month. Events 3 and 4 had  
347 less rainfall and dilution of EC was less (from about 1300 to about 800  $\mu\text{S}/\text{cm}$ ) and recovery took more than one and a half  
348 month in event 3, during which multiple small events occurred. The dilution patterns of the NH<sub>4</sub> in events 1 and 2 were similar  
349 to those of EC ( $R^2 = 0.86$  and  $0.83$ , respectively, Table S7 & S8) and show resemblance for event 3 ( $R^2 = 0.75$ , Table S10).  
350 Moreover, a direct negative correlation between NH<sub>4</sub> and rain intensity supports this dilution effect for event 2. Due to the data  
351 gaps of NH<sub>4</sub> in event 4 we cannot completely describe the pattern of NH<sub>4</sub> for this one, but it corresponds with that start of  
352 reduced NH<sub>4</sub> which was described in sections 3.1 and 3.2.

353 The response of TP was generally not related to the intensity of rainfall and pumping, except for event 3 during the wet period.  
354 Dilution effects, as were observed for NH<sub>4</sub>, were not observed for TP for events 1, 2 and 4. During the wet season event 3, TP  
355 concentrations show negative correlations with precipitation and pumping intensity ( $R^2 = -0.79$  and  $-0.59$ , respectively, Table  
356 S9) and correspond with decreasing turbidity. Event 4 marks the transition between the wet and dry season and the drop in TP  
357 coincides with the drop in NH<sub>4</sub>, independently from individual rain storms during the dry season.

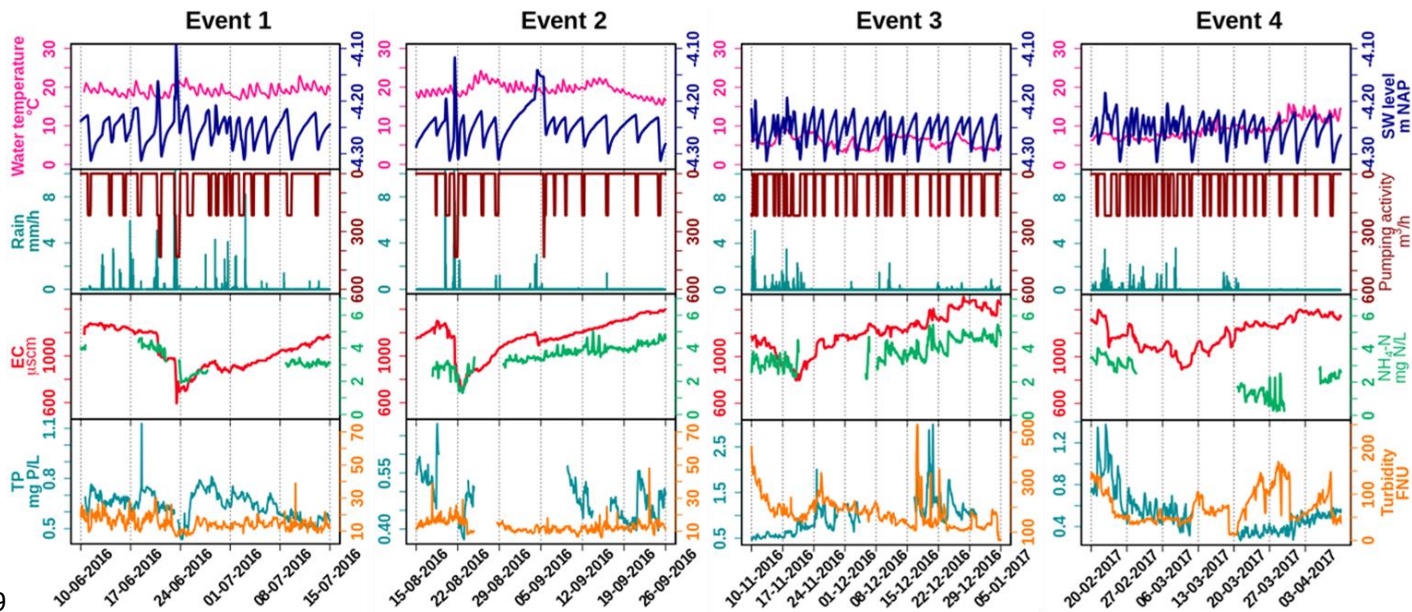
358 During the dry season (with event 1 and 2 included) turbidity always stayed below 50 FNU. Turbidity sometimes showed  
359 single peaks which are likely related to disturbances of the floating platform by wind and should probably be treated as false  
360 signals. Turbidity is more variable and has higher variance for wet season events 3 and 4, which corresponds with the findings  
361 of the annual scale analysis (section 3.1.2). During event 3, turbidity varied between 100 and 500 FNU. Although clear relations  
362 exist between Fe, TP and turbidity, all higher during the wet season (Figure 2, Table S2), these are not clearly reflected at the  
363 scale of individual precipitation events. Simultaneous peaks of TP and turbidity occur that are not easily related to the weather  
364 conditions in November and December but TP and turbidity show contrasting signals at the start of the event. The turbidity  
365 clearly decreases during rain storm event 3 and at the start of event 4. This change is not reflected by the correlation at the total  
366 event scale (Tables S9 and S10) but obvious when studying only the time scale of the decreasing limb of the EC dilution.  
367 Event 4 coincides with the transition to the spring season in 2017, showing decreasing EC, TP and turbidity in the last rains of  
368 the wet season and a strong decrease of NH<sub>4</sub> and increase of turbidity when conditions dried up and temperatures rose.

#### 369 3.3.2 Pumping events and day and night pattern

370 The selected pumping events covered four seasons: summer (2016 July, event 1), autumn (2016 October, late autumn, event  
371 2), winter (2016 December, event 3) and spring (2017 May, event 4) (Fig.5). While the effects of pumping on EC are rather  
372 small, TP, NH<sub>4</sub> and turbidity are all affected by pumping. The effects of pumping appear to be different for events in different  
373 seasons; turbidity for example increases during pumping in July and December but decreases in May. The increase during the  
374 December pumping is especially marked ( $R^2$  Pumping intensity versus Turbidity =  $0.77$ , Table S13). TP decreases during  
375 pumping in July ( $R^2 = -0.67$ ) and October and increases in May ( $R^2 = 0.6$ ). Event 2 seems to have started a major drop in  
376 turbidity (more than 1000 FNU) that continued some time after pumping.

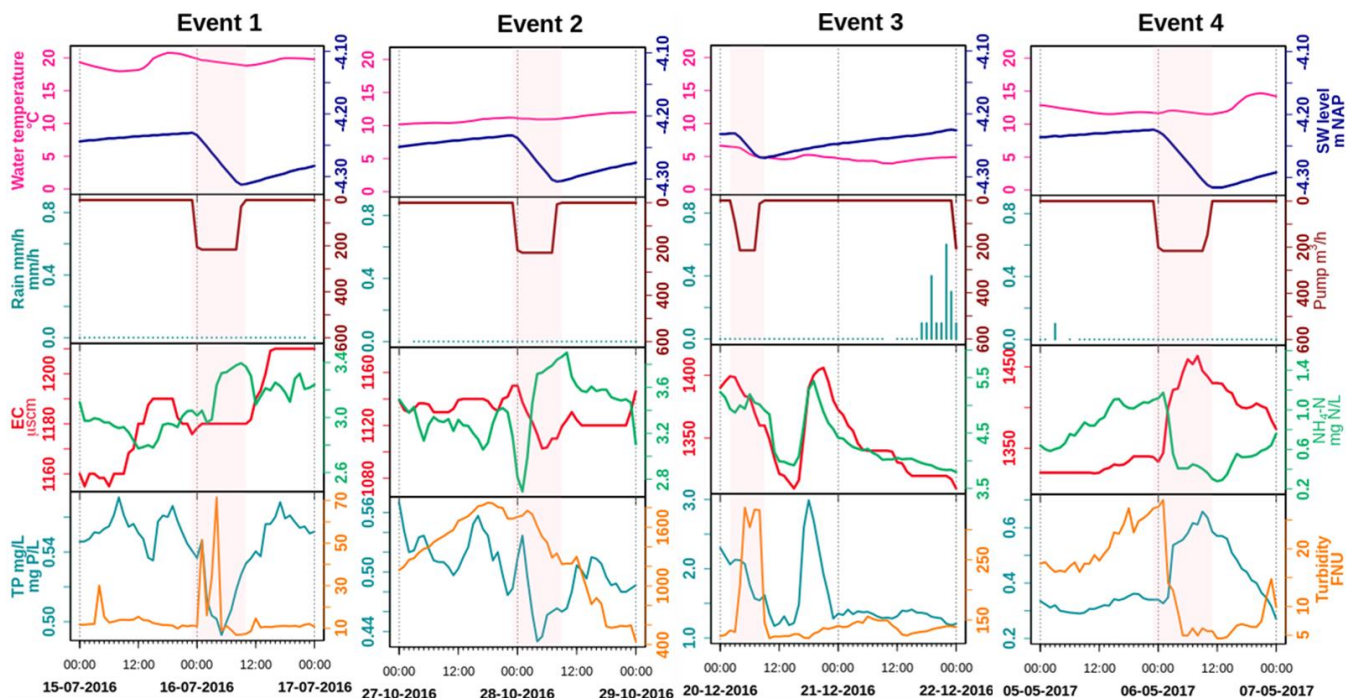
377





379

380 **Figure 4** Selected events showing dilution and peaks of water quality parameters, with hourly precipitation (mm/h)  
 381 and hourly pumping activity (m<sup>3</sup>/h). Note that between events different scales of TP and turbidity were used to reveal  
 382 the dynamics. See Table S7-S10 for the correlation tests performed on the dataset.  
 383



384

385 **Figure 5** Pumping and pumping effect patterns on water quality, blue blocks represent the pumping duration. See  
 386 Table S11-S14 for the correlation tests performed on the dataset.

#### 387 4. Discussion

388 This study aimed at understanding the dynamics of N and P fluxes from the low-lying urban polder of Geuzenveld to  
 389 downstream surface waters in order to eventually support water managers to mitigate eutrophication. Based on our high-  
 390 resolution water quality measurements, we found that the surface-water chemistry at the polder outlet pumping station is  
 391 governed by a complex combination of hydrological mixing and biogeochemical processing. In the following discussion, we  
 392 start with the presentation of the relatively straightforward dilution behavior of EC, followed by adding the impact of primary  
 393 production (i.e. algae growth) for understanding the NH<sub>4</sub> concentration patterns, and benthic primary producer and iron  
 394 chemistry for understanding the turbidity and TP concentration patterns.

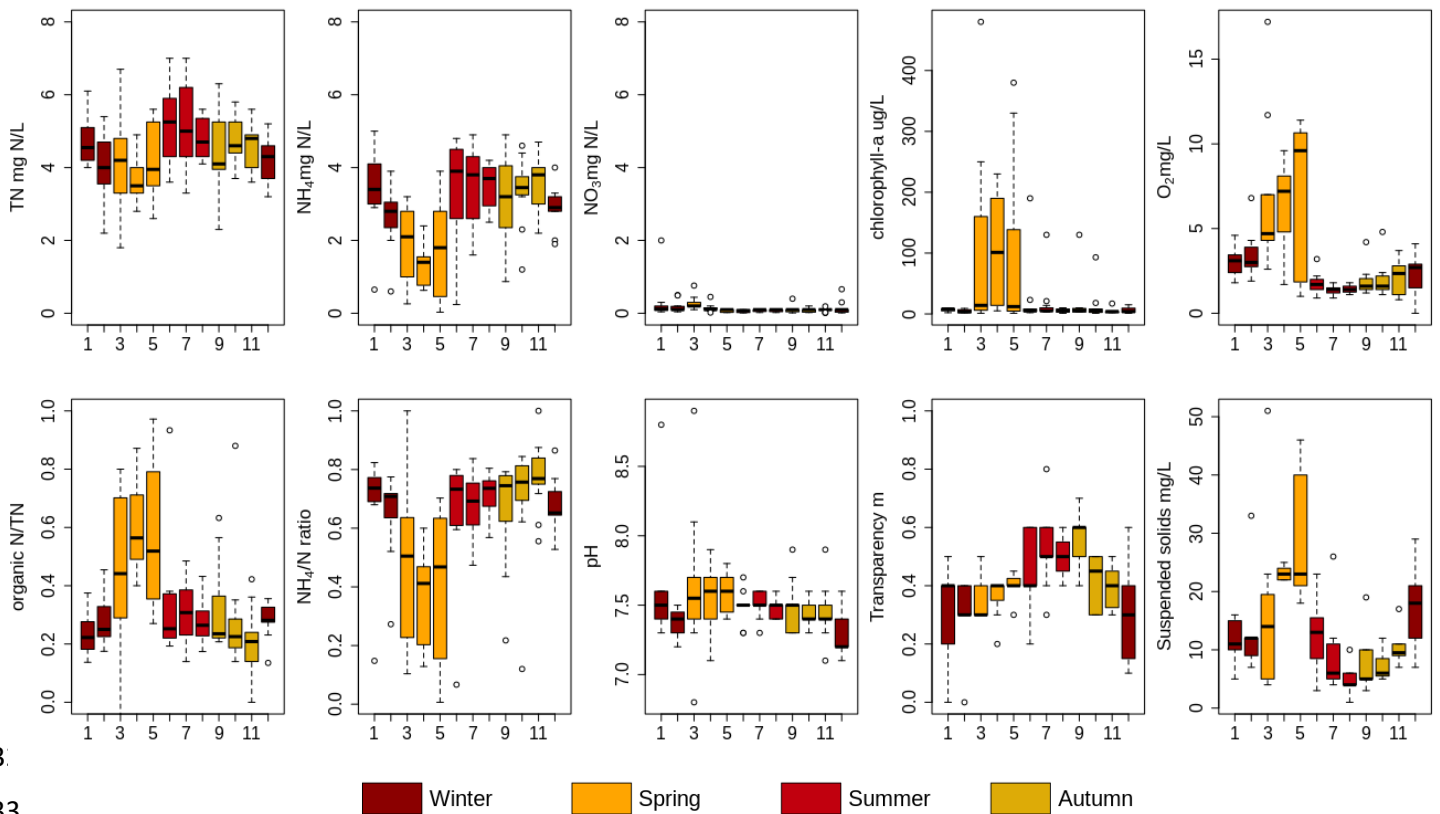


#### 395 4.1 Hydrological mixing between groundwater and rainfall

396 In a highly manipulated low-lying urban catchment like Geuzenveld, mixing between rainwater and groundwater in the ditches  
397 is fast due to the high fraction of impervious area and the installation of both a rainwater and a groundwater drainage system  
398 that transport these contrasting water types efficiently to the ditches (Yu et al., 2019; Walsh et al., 2005). Runoff in Geuzenveld  
399 has EC of about 166  $\mu\text{S}/\text{cm}$  (Yu et al., 2019), which is lower than the groundwater EC (1746  $\mu\text{S}/\text{cm}$  on average). As a relatively  
400 conservative water quality parameter (Figure S2), mixing between rainwater and groundwater should be the main process for  
401 EC. This presumption is supported by the agreement between the modelled and the measured EC dynamics for the period  
402 between May to November 2016. Precipitation events diluted the EC values at the pumping station, and the magnitude of  
403 dilution depended on the intensity of precipitation; heavy rainfall resulted in low EC values (Fig.2D and Fig.4). In periods  
404 with the absence of rainfall, the EC values follow a recovery curve that resembles a linearly mixed reservoir with  
405 concentrations increasing to values that approach the EC of the continuous groundwater supply of around 1500  $\mu\text{S}/\text{cm}$ . After  
406 November 2016, EC was underestimated by the model. The sudden increase of the measured EC around Nov 20<sup>th</sup> coincides  
407 with an intensive pumping event after the first intensive rainfall that happened after a prolonged period of cumulative water  
408 deficit. This may be related with a first flush from the drain system that starts to be activated more strongly, thus removing  
409 clogged material and lowering the overall resistance of the drain system for shallow and deep groundwater inflow (van der  
410 Velde et al., 2010). It suggests that this triggered the inflow of somewhat more mineralized groundwater relative to the period  
411 before, creating a shift in the EC towards  $\sim 250$   $\mu\text{S}/\text{cm}$  higher values that continued during the remainder of the monitoring  
412 campaign. It appeared that it raised the EC, but did not change its amplitude or dynamics during the remainder of that period  
413 (Fig. 2 and 3, Table S6). The elevated EC may alternatively due to the application of road salts in winter which starts from  
414 November. But we did not find any evidence for the prolonged effects of road salts, as the chloride concentrations in the grab  
415 samples only showed two higher measurements, one in December 2016 and one in January 2017 (see Supplement, Figure S2).  
416 The mixing process can explain part of the dynamics of  $\text{NH}_4$  and TP in the wet season, but insufficient for explaining the  
417 dynamics during the dry season due to the presence of biological and chemical processes. Compared with groundwater, which  
418 carries around 8  $\text{mg L}^{-1}$   $\text{NH}_4$  and 1.6  $\text{mg L}^{-1}$  TP, rain and runoff have much lower nutrient concentrations, which makes  
419 groundwater the main nutrients source (Yu et al., 2019). Nutrients derived from groundwater mix with rainwater in the ditches  
420 through direct seepage and the efficient groundwater drainage systems. Clearly,  $\text{NH}_4$  is diluted during the rain events and a  
421 gradual increase of  $\text{NH}_4$  starts after each rain event during the wet season showing slopes that resemble the model  
422 reconstruction. The overestimation of the modeled  $\text{NH}_4$  in general indicates a probable lost to transformation processes,  
423 especially in the spring of 2017. Concentrations of TP are also generally far below the conservative model reconstruction. The  
424 distinct peaks up to 3  $\text{mg L}^{-1}$  are not captured by the model and must be determined by different physical or chemical processes.

#### 425 4.2 Primary production and nutrients

426  $\text{NH}_4$  dynamics during winter can be explained by mixing. However, biological processes are overruling the mixing process  
427 during spring and summer. It resulted in lower measured  $\text{NH}_4$  concentrations than modeled during this period. Studies have  
428 shown that benthic and planktonic primary producers (e.g. phytoplankton) assimilate nutrients and are an important factor  
429 controlling nutrient dynamics in rivers, lakes, and streams (Hansson, 1988; Jäger et al., 2017). In polder Geuzenveld, the  
430 biological nutrient uptake is not only reflected in the time series data (Fig.2 and 3, Table S3) but is also evident in the monthly  
431 measurements from the water authority for the period 2007-2018, as summarized in Figure 6 and Table S15-S19.



43

433

434

435

436

**Figure 6 Monthly measurements of TN, NH<sub>4</sub>-N, NO<sub>3</sub>-N, chlorophyll-a, O<sub>2</sub> organic N/ TN and NH<sub>4</sub>-N/TN (NH<sub>4</sub>/N) mass ratio, pH, water transparency, and suspended solids in Geuzenveld from 2007 to 2018. X axis is month. See Table S15-S19 for the correlation tests performed on the dataset.**

437

438

439

440

441

442

443

444

445

446

447

448

449

450

451

452

453

454

455

456

457

458

The increasing availability of light (and temperature increase) during spring (Figure S6), induces growth of primary producers. Growth of primary producers results in consumption of ammonium, phosphate and a production of organic-N, chlorophyll-a, oxygen, and suspended solids, and led to a relatively higher pH because of the uptake of CO<sub>2</sub> (Figure 6, Table S16). These patterns are also clearly reflected in the shift in the NH<sub>4</sub>/TN and organic-N/TN ratios during spring (Figure 6). Primary production occurs both in the water column by phytoplankton as well as by benthic algae. Macrophytes could in principle also contribute, but they were absent in Geuzenveld. One of the structuring factors governing the relative importance of benthic and planktonic primary producers is light availability: benthic algae and macrophytes tend to dominate in shallow and clear waters, while phytoplankton is more likely to dominate in deeper and more turbid waters (Hartwig, 1978; Jäger and Borchardt, 2018; Petranich et al., 2018; Middelburg, 2019). Although our data do not allow conclusive determination whether benthic or pelagic primary producers dominate, it appears that their relative importance varies with season.

These primary producers also compete for nutrients. Benthic primary producers have direct (macrophytes) or first (benthic algae) access to nutrients that seep up from the subsurface, while planktonic primary producers depend on nutrient supply from surface runoff and nutrients remaining after consumption by benthic primary producers. For example, Henry and Fisher (2003) found that benthic algae can remove up to 80% of nitrogen from an upwelling water source. As we stated above, nutrient-rich groundwater is the major source of N and P to surface waters in polder Geuzenveld. In addition, due to the shallow depth of the ditches, light reaches the bottom with the consequence that benthic algae can proliferate in this polder. These benthic primary producers might utilize the up-flowing nutrients from groundwater and intercept the nutrients from seeping further into the water column (Hansson, 1988; Pasternak et al., 2009). The increasing light availability and thus primary production during spring led to the nearly complete deprivation of NH<sub>4</sub> in the water column (Fig.2C).

Following the spring bloom, concentrations of chlorophyll-a (proxy for phytoplankton biomass) and O<sub>2</sub> dropped substantially, while NH<sub>4</sub> concentrations rapidly recovered to around 4 mg L<sup>-1</sup> in both the time series (Fig.2C) and the long-term monthly

459 sampling results (Fig.6). Dissolved O<sub>2</sub> remained low (close to hypoxia) during the whole summer (below 2 mg L<sup>-1</sup>) (Fig.2E  
460 and Fig.6), indicating that oxygen consumption by organic matter degradation and re-oxidation of reduced components from  
461 groundwater seepage outcompeted oxygen production from primary production. During summer, suspended solid and  
462 chlorophyll-a concentrations were low (Fig.6), indicating low biomass of plankton algae. Suspended solid and phytoplankton  
463 dominate light attenuation (Scheffer, 1998; Middelburg, 2019). Consequently, during this period, we observed an abrupt shift  
464 of the water regime from a turbid state to completely clear, as reflected in the high transparency from June to September (Fig.  
465 6). The low biomass of phytoplankton might be due to N limitation as nutrients are intercepted by benthic algae at the sediment  
466 interface. An alternative explanation is that zooplankton grazing maintained phytoplankton biomass low (Strayer et al., 2008;  
467 Genkai-Kato et al., 2012).

468 Temperature and light reaching the sediment started to fall from September onwards (Figure S6), thereby reducing the intensity  
469 of biological activity, including NH<sub>4</sub> assimilation. Consequently, NH<sub>4</sub> started to behave conservatively again like EC (Fig.2 &  
470 Fig.3). The best fit between the modeled and measured NH<sub>4</sub> was from the end of November to the beginning of March, i.e  
471 during the winter period with lower light levels and shorter day lengths and very low primary production. The absence of  
472 primary production during winter, leads to conservative behavior of NH<sub>4</sub> governed by the mixing between groundwater and  
473 rain water.

474

#### 475 **4.3 P binding and turbidity**

476 Iron chemistry is considered the dominant process governing the P dynamics in shallow groundwater fed ditches (Lijklema,  
477 1994; Smolders et al., 2006; van der Grift et al., 2018). However, primary producers take up P for growth and at the same time  
478 release O<sub>2</sub> that regulates iron chemistry in lake water column (Table S1-S3, Spear et al., 2007; Zhang and Mei, 2015; Lu et al.,  
479 2016). This web of interactions likely controls P dynamics in these ditches.

480 From spring to autumn, TP concentrations were fluctuating around 0.5 mg L<sup>-1</sup>, and the water had low turbidity (<50 FNU),  
481 thus high transparency allowing the growth of benthic algae that produce oxygen. Consequently, when P and Fe rich anoxic  
482 groundwater reaches the surface water-sediment interface, Fe oxidized into iron hydroxides in a short time (Van der Grift et  
483 al., 2014). P is then sorbed onto those Fe-hydroxides and retained in the sediments. Oxidation of reduced iron consumes O<sub>2</sub>,  
484 contributing to the low O<sub>2</sub> conditions of the water column (Fig.2E). Moreover, it leads to the formation of a reddish-brown  
485 film of ferric iron (hydrated ferric oxide, Baken et al., 2013; van der Grift et al., 2018) on the bottom of the ditches, which can  
486 be seen in summer when the water was transparent. This slimy layer comprising iron hydroxides and benthic microbes can  
487 easily be resuspended and therefore act as a source of turbidity following perturbations by pumping, wind, rain or foraging  
488 fish, e.g. event 1 (Fig.5). Lu et al (2016) showed that co-precipitation of P with metal oxides was stimulated by periphytic  
489 biofilm activity that increased the water pH. Consistently, a relatively higher pH was also observed in our spring monthly  
490 samples (Fig.6).

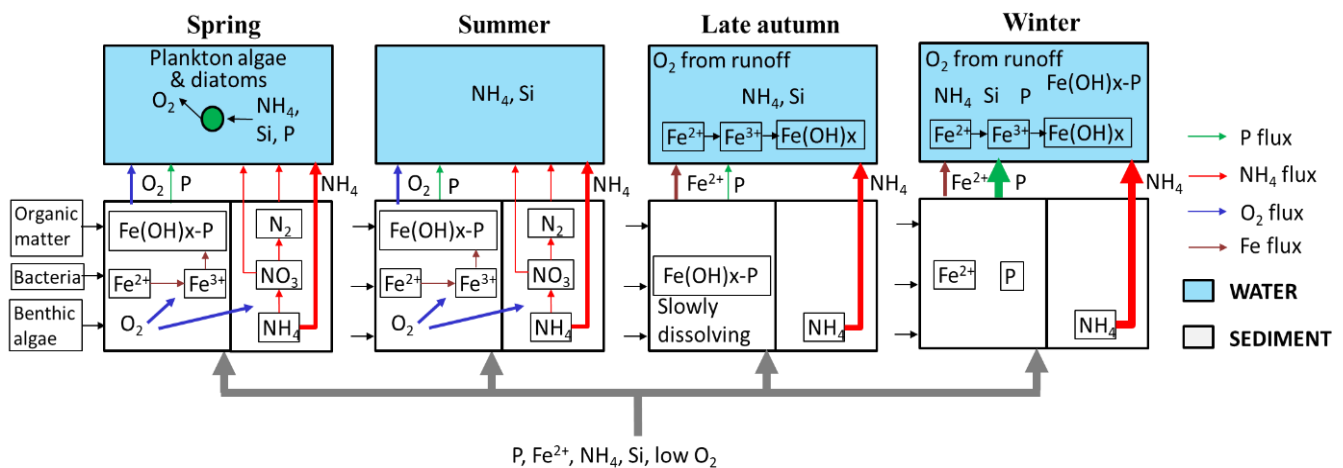
491 From the late autumn onwards, turbidity and total Fe concentrations substantially increased compared to the rest of the time  
492 (Fig.2, p value < 0.001 for turbidity and = 0.02 for Fe). Turbidity peaked first at 1800 FNU and stayed at a plateau of ~200  
493 NFU during the rest of the cold and wet season. Total Fe in the water column reached to 6 mg L<sup>-1</sup> from below 1 mg L<sup>-1</sup>. During  
494 this period the water turned brownish and transparency declined (Fig.6). Iron-rich particles are the most likely source of  
495 turbidity in freshwater (Lyvén et al., 2003; Gunnars et al., 2002; and Lofts et al, 2008). The suspension of these brownish iron  
496 colloids was likely stabilised by the presence of the dissolved organic matter (Mosley et al., 2003; Van der Grift et al., 2014),  
497 which (DOC) increased up to 18~33 mg L<sup>-1</sup> during events (Supplementary information Figure S4). In the late autumn, the  
498 anoxic/oxic interface shifts from the sediment into the water column and so does the locus of colloid formation. The ditch  
499 sediment, which had benthic algae activity releasing O<sub>2</sub> during spring and summer, became anoxic in the fall by the upwelling  
500 of the anoxic groundwater. The anoxic seepage occurs year-round, but the production of oxygen by the benthic algae creates  
501 an anoxic-oxic transition at the water-sediment interface, which leads to iron hydroxides precipitation in the slimy layer at the

502 bottom that disappears after the algae die off. As a consequence, Fe oxidation moved into the water column where the  
 503 conditions were relatively oxic (Van der Grift et al., 2014). Nevertheless, there was probably still enough Fe or other mineral  
 504 oxides, such as aluminum hydroxide (Kopáček et al., 2005), binding capacity in the sediment for the fixation of P, as P  
 505 concentrations remained low during this first turbidity peak. We suggest that the turbidity peak of 1800 FNU is caused by the  
 506 mineralisation of the benthic algae once they die off when light and temperature conditions decrease, combined with the shift  
 507 of ironhydroxide formation from the sediment-water interface to the water column. The latter process continues through the  
 508 whole winter season, until primary production restarts in spring (Figure 7).

509 During winter, temperatures were below 5°C, pH values were relatively lowered, and TP achieved its peak concentrations  
 510 (Fig.2D). During this period, iron reduction in the sediments continued, P bounded to iron oxides gradually got released along  
 511 with reduced iron (Li et al., 2016). In the water column, reduced iron was oxidized but much slower than during spring-autumn  
 512 due to the lower temperatures (Van der Grift et al., 2014), and dissolved P was incorporated in iron flocs with the result that  
 513 particulate P concentrations and turbidity became high (Table S1, R<sup>2</sup> for Fe~turbidity 0.81, TP~Fe 0.65; Table S2, Fe~turbidity:  
 514 R<sup>2</sup> = 0.72, , TP grab~Fe 0.79; Yu et al., 2019).

#### 515 4.4 Process synthesis

516 With the presence of benthic algae, abundant organic matter and bacteria, the sediment functions as an active environment for  
 517 biotic processes (such as primary production and nitrification-denitrification-anammox) and abiotic processes (such as iron  
 518 oxidation). Figure 7 shows a conceptual diagram for the N and P dynamics in this lowland urban catchment during the four  
 519 seasons which summarizes our hypotheses about the functioning of the system.



520 P, Fe<sup>2+</sup>, NH<sub>4</sub>, Si, low O<sub>2</sub>

521 **Figure 7 Schematic representation of N and P dynamics in spring, summer, later autumn and winter. The thickness of the flow lines**  
 522 **represents the concentration magnitudes, the thicker the line, the higher the concentrations.**  
 523

524 **Spring:** The improved light (and temperature) conditions stimulated primary production and nutrient uptake (N, P, Si) by  
 525 phytoplankton and benthic algae. The resulting oxygen production caused oxidation of reduced iron from groundwater and the  
 526 formation of iron oxides at the sediment surface. P was mostly bounded to this particulate iron instead of being released into  
 527 the upper water layer. In this period turbidity was relatively low, but suspended solids reached a high concentration due to the  
 528 phytoplankton.

529 **Summer:** N and P were still being removed by biological processing, in particular by benthic algae. Phytoplankton biomass  
 530 decreased because of competition for N or grazing activity. Benthic algae produced O<sub>2</sub>, which in turn was used to oxidize all  
 531 reduced iron reaching the sediment-water interface and P was still retained by iron hydroxides in the sediment. The water  
 532 column was transparent (low TP and phytoplankton biomass) and relatively low in oxygen due to the continuous supply of  
 533 anoxic groundwater, the mere absence of O<sub>2</sub>-rich runoff, the oxidation process of Fe(II) and possibly by microbial organic  
 534 matter decomposition during warm periods with relatively stagnant water.

535 **Late autumn:** Biological activity declined (colder and less light), and more  $\text{NH}_4$  reached the water column. Moreover, the  
536 redox zone moved from the sediment-water interface into the water column (Van der Grift et al. 2014, 2016); the oxidation of  
537 Fe in the water column caused a peak of turbidity. P was still sequestered to minerals in the sediment.

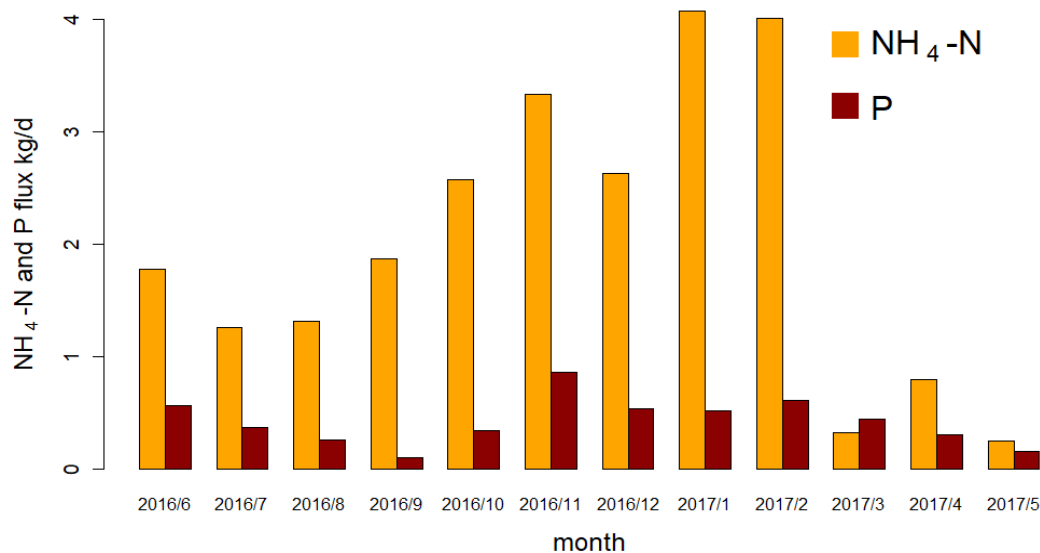
538 **Winter:** During winter,  $\text{NH}_4$  and TP showed the highest concentrations because of low biological activity. Iron oxides in the  
539 sediment dissolved under reductive and organic matter abundant conditions and released  $\text{Fe}^{2+}$  and P into the water column  
540 increasing P concentrations therein.  $\text{NH}_4$  and EC dynamics were primarily governed by the conservative mixing between  
541 groundwater and precipitation/runoff.

#### 542 **4.5 Event scale N and P dynamics**

543 At the event scales,  $\text{NH}_4$  and EC were reduced by dilution from precipitation/runoff. For P and turbidity there was no clear  
544 relation to precipitation events, except for events in late autumn and winter (e.g. Figure 4, event 3). The responses to  
545 precipitation and pumping events were different from those reported in the literature. Rozemeijer et al. (2010b) studied an  
546 agricultural catchment and found that rainfall events led to  $\text{NO}_3$  decreases and P increases. Miller et al. (2016) observed  $\text{NO}_3$   
547 decreases during large discharges in an urban catchment. The lowering of turbidity in our urban catchment during the dilution  
548 periods that was associated with the winter events 3 differs from the observations in literature (van der Grift et al., 2014,  
549 Rozemeijer et al., 2010b). In agriculture areas, turbidity usually peaks in response to rainfall events due to erosion and  
550 remobilization of sediments. In an urban, paved environment erosion may be limited and runoff water has a low turbidity.  
551 Moreover, in the case of turbid pre-event conditions, fresh precipitation water flushes away this turbid water. In addition, Yu  
552 et al. (2019) showed that precipitation runoff delivers particles and  $\text{O}_2$  to the ditches. We suggest that this accelerates the  
553 further aggregation of the iron complexes; the resulting larger particles more readily settle to the bottom, causing a reduction  
554 of turbidity during the events itself (Fig. 4, EC dilution part of events 3 and 4).

555 In artificial lowland catchments, water systems are intensively regulated by pumping activity to prevent flood and drought.  
556 However, there is a substantial lack of knowledge about the possible consequences of such regulation on aquatic ecology and  
557 water quality. Peaks in P and turbidity by the activation of pumps was observed by Van der Grift et al. in their high frequency  
558 monitoring campaign in an agriculture lowland polder (Van der Grift et al., 2014 & 2016). This type of event scale dynamics  
559 would be easily missed in a daily or lower frequency sampling schedule, especially because pumping occurs almost solely  
560 overnight in our regulated catchments. As such, only a sampling schedule with 7 hours intervals (e.g. Neal et al. 2011) or high-  
561 frequency monitoring is able to catch the short-term dynamics (Van Geer et al. 2016).

562 Contrary to the findings of Van der Grift et al. (2014, 2016), the effects of pumping activity on N, P and turbidity dynamics  
563 were variable, depending on the season. During the phytoplankton bloom in spring, activation of pumps resulted in flushing  
564 and as a result reduced turbidity during the event (Fig. 5 event 4). Consequently, phytoplankton was transferred to the  
565 downstream channel and added to the total N pool in that system. In summer (Fig.5 event 1), the dead detritus and the layer of  
566 iron compounds at the sediment surface were easily resuspended and contributed to turbidity peaks at the beginning of the  
567 pumping, but the materials also re-sedimented almost immediately once the flow reached stability. Resuspension also resulted  
568 in an increase of  $\text{NH}_4$  in the water column which then was being pumped out (Fig.5 event 1). During late autumn, we observed  
569 that the water was highly turbid (see also Yu et al. 2019) which we suggest to be caused by the formation of iron hydroxide  
570 colloids in the water column, which is supported by correlations between Fe-grab and Turbidity ( $R^2= 0.72$ , Table S2). We  
571 explain the reduced turbidity after a precipitation event as a result of the activation of the pumps which caused the export of  
572 the turbid water towards the receiving boezem in combination with aggregation of iron hydroxides in the water column and  
573 subsequent settling of the aggregates due to the supply of new  $\text{O}_2$ -rich water (Fig.5 event 2, see also Van der Grift, et al., 2014).  
574 Moreover,  $\text{NH}_4$  increased again by the pumping activity and was transferred downstream (Fig.5 event 2). The eventual impact  
575 of regulation of the Geuzenveld water system turns the pumping discharge into a point source for nutrients to downstream  
576 water bodies as shown in Figure 8.



577

578 **Figure 8 Average daily NH<sub>4</sub>-N and P flux (kg per day) in each month in the discharge (calculated from the continuous**  
 579 **measurements) of polder Geuzenveld from June 2016 to May 2017.**

580

581 Fluxes of N and P were highest during winter (Fig 6). These high fluxes are caused not only by the more frequent pumping  
 582 activity, but also by the higher concentration of N and P in the water column in winter. In the time series data, NH<sub>4</sub> (the major  
 583 form of N), had concentrations above 2.4 mg N L<sup>-1</sup> (the local environmental quality standard (EQS) for N-total), in all seasons  
 584 except spring. NH<sub>4</sub> concentrations even reached up to 6.5 mg L<sup>-1</sup>. TP concentrations were constantly higher than 0.15 mg P L<sup>-1</sup>  
 585 (the local EQS); during winter it was always over 1 mg P L<sup>-1</sup>. Although the NH<sub>4</sub> flux in the discharge was very low in spring  
 586 (Fig.8), the actual total N flux might have been much higher, as organic N (phytoplankton) was the major form of TN instead  
 587 of NH<sub>4</sub> during this period (Fig.6 NH<sub>4</sub>/N and organic-N/TN). Therefore, even though water authority measures have been  
 588 effective in controlling the water quantities in the polder, it had unanticipated impact on nutrients export to the downstream  
 589 water bodies. In order to prevent eutrophication in the urban waters, nutrient rich discharge from these areas is exported directly  
 590 to the North-Sea Canal and to the North Sea.

591

#### 592 **4.6 Implications for urban water management in low lying catchments**

593 This study demonstrated high frequency monitoring technology to be an effective tool for understanding the complex water  
 594 quality dynamics. Investment in high frequency monitoring would greatly benefit the management of urban lowlands with  
 595 substantial groundwater seepage by elucidating the principle biogeochemical processes and nutrient temporal patterns for  
 596 realizing efficient mitigation and control of eutrophication. For example, redirecting the drain water effluent into constructed  
 597 wetlands could be considered as a mitigation measure in low lying areas with artificial water systems that resemble the  
 598 Amsterdam region, e.g. in cities such as New Orleans, Shanghai and Dhaka (Li et al., 2009; Nahar et al., 2014; Jones et al.,  
 599 2016; Stahl, 2019). Centralizing the treatment of discharge water is also recommended, for instance by harvesting N as  
 600 phytoplankton from the discharge during spring, or filtrating P at the pumping station during winter. Measures that artificially  
 601 increase oxygen concentrations in the waters, such as the inlet of oxygen rich water, aeration by fountains or the artificial  
 602 introduction of grazers or macrophytes may be considered to improve the ecological status of these urban waters. Moreover,  
 603 aeration of the water in summer and autumn would possibly enhance processes such as coupled-nitrification-denitrification  
 604 and anammox, eventually converting NH<sub>4</sub> to N<sub>2</sub>, before the water is discharged to downstream waters. Importantly, before the  
 605 application of any measures or maintenance in urban low-lying catchments, managers should evaluate the potential effects on



606 the biological and chemical resilience, e.g. dredging of a layer with abundant benthic activity might destroy an important buffer  
607 to nutrients in growing seasons, especially P.

608 In this study, we focused on the analysis of the temporal patterns of water composition and on the deduction of the potential  
609 biogeochemical processes. Detailed studies about these processes and the biotic communities at the sediment-water interface  
610 were outside of the scope of this paper. A comprehensive study on the sediment-water interface would be necessary to further  
611 increase our knowledge on the role of the benthic zone in attenuating N and P seeping up from groundwater. Besides, further  
612 research would need to consider the optimal physical dimensions of water courses and drain configurations, as to benefit the  
613 ecological status of urban waters that are prone to nutrient-rich groundwater seepage.

614

## 615 **5. Conclusions**

616 This study aimed at improving our understanding of the mechanisms that control the temporal patterns of nutrients and other  
617 water quality parameters in an urban catchment. Time series of EC, NH<sub>4</sub>, TP, and turbidity were obtained by applying a high  
618 frequency monitoring technology for one year (May 2016 to July 2016). Observed EC, NH<sub>4</sub> and TP could only partly be  
619 explained by conservative mixing of groundwater and precipitation components. In particular, N and P fluxes in the shallow  
620 ditches were also impacted by biogeochemical processes, such as primary production and iron redox transformations.

621 (1) NH<sub>4</sub>, the dominant form of N in surface water, originates primarily from groundwater seepage, and concentrations  
622 are lowered by primary producers (phytoplankton and benthic algae) in the growing season. High algal biomass was  
623 also clear from high chlorophyll-a and suspended solids in the water column.

624 (2) TP showed high concentrations in winter, but relatively low concentrations in other seasons. Iron redox chemistry  
625 was the principle process controlling the P dynamics in shallow groundwater fed ditches. P dynamics may also have  
626 been partly influenced by primary production which consumes P for growth and at the same time produces O<sub>2</sub>  
627 influencing the redox status in the sediments and in the water column.

628 (3) High turbidity levels occurred in the late autumn and winter, mostly in the form of iron hydroxides. It resulted from  
629 a shift of the anoxic/oxic interface where the formation of iron hydroxides moves from the sediment towards the  
630 water column.

631 (4) Water pumped from the polder to downstream water bodies was rich in NH<sub>4</sub> from summer to winter, but rich in  
632 organic N in the form of algae during spring. P leaves the polder mainly during the winter season when it is released  
633 from the sediment and exported mostly in the form of P sorbed to Fe(OH)<sub>3</sub> colloids and as dissolved P.

634 (5) Precipitation diluted concentrations of most water quality parameters, but delivered O<sub>2</sub> to the water column, and in  
635 that way indirectly affected P and turbidity by intensifying iron oxidation and precipitation.

636 (6) Unlike many other natural and artificial catchments, rainfall and pumping events did not increase turbidity or TP  
637 concentrations at the short time scale, rather reduced turbidity and TP because of enhanced iron hydroxide  
638 precipitation due to oxygen inputs by runoff.

639 Our understanding of the N and P dynamics in this low-lying urban catchment may contribute to the development of effective  
640 water management strategies that reduce eutrophication conditions in both the urban polders and the downstream waters.  
641 Drainage of very low-lying areas (for use as residential and/or agricultural areas) not only increases pumping costs, but can  
642 also result in difficult to manage water quality conditions. Controlling the source, redirecting and utilizing the drainage water  
643 might be strategies to reduce the input of N and P from groundwater into surface water. In addition, we showed that in lowland

644 urban areas with high seepage rates the reactivity of the stream bed sediments largely controls water quality of surface waters  
645 and thus should be managed with care when cleaning the surface water systems.

## 646 **Acknowledgements**

647 This work was funded through China scholarship council (no. 201309110088) and supported by Waternet, the Strategic  
648 Research Funding of TNO and Deltares. We highly appreciate the help and support from our Waternet co-workers: Eelco  
649 Wiebenga, Henk Molenaar, Sonja Viester, Laura Moria, and Frank Smits.

650 **Code/data availability:** The code scripts and datasets related to this paper are available on request to Liang Yu, contact is  
651 xiaobaidrawing@gmail.com.

652

653 **Author contribution:** Maarten Ouboter, Joachim Rozemeijer, and Hans Peter Broers funded this research. Hans Peter Broers  
654 and Joachim Rozemeijer designed the field work. Liang Yu carried out the field work and the data collection, analysis,  
655 visualization, discussion, and the writing of the manuscript, under the supervision of Hans Peter Broers and Joachim  
656 Rozemeijer before 2019, Ype van der Velde as the main supervisor since 2019. All the authors participated the discussion of  
657 the data analysis results, and helped prepare the manuscript.

658

659 **Competing interests:** The authors declare that there is no conflict of interest.

## 660 **References**

661 Audet J., Zak D., Bidstrup J., and Hoffmann C.C.. Nitrogen and phosphorus retention in Danish restored wetlands. Royal  
662 Swedish Academy of Sciences, 1-13, 2019.

663 Bunch N.D. and Bermot M.J.. Nitrate and ammonium uptake by natural stream sediment microbial communities in response  
664 to nutrient enrichment. *Research in Microbiology*, 163(2): 137-141, 2012.

665 Beusen A.H.W., Bouwman A.F., van Beek L.P.H., Mogollón J.M., and Middelburg J.J.. Global riverine N and P transport to  
666 ocean increased during the 20th century despite increased retention along the aquatic continuum. *Biogeosciences*. 13: 2441-  
667 2451, 2016.

668 Bierozza M.Z., Heathwaite A.L., Bechmann M., Kyllmar K., and Jordan P.. The concentration-discharge slope as a tool for  
669 water quality management. *Science of the Total Environment*, 630: 738-749, 2018.

670 Baken S., Sjostedt C., Gustafsson J.P., Seuntjens P., and Desmet N.. Characterisation of hydrous ferric oxides derived from  
671 iron-rich groundwaters and their contribution to use suspended sediment of streams. *Applied Geochemistry*, 39: 59-68, 2013.

672 Cavaliere E. and Baulch H.M.. Winter nitrification in ice-covered lakes. *PLoS ONE*, 14(11): e0224864, 2019.

673 Chen M., Ding S., Chen X., Sun Q., Fan X., Lin J., Ren M., Yang L., and Zhang C.. Mechanisms driving phosphorus release  
674 during algal blooms based on hourly changes in iron and phosphorus concentrations in sediments. *Water Research*, 133: 153-  
675 164, 2018.

676 Díaz P., Stanek P., Frantzeskaki N., and Yeh D.H.. Shifting paradigms, changing waters: Transitioning to integrated urban  
677 water management in the coastal city of Dunedin, USA. *Sustainable Cities and Society*. 26: 555-567, 2016.

678 Duncan J.M., Welty C., Kemper J.T., Groffman P.M., and Band L.E.. Dynamics of nitrate concentration-discharge patterns in  
679 an urban watershed. *Water Resources Research*, 53: 7349-7365, 2017.

680 Eggimann S., Mutzner L., Wani O., Schneider M.Y., Spuhler D., de Vitry M.M., Beutler P., and Maurer M.. The Potential of  
681 Knowing More: A Review of Data-Driven Urban Water Management. *Environmental Science & Technology*, 51: 2538-2553,  
682 2017.

683 Filippelli M.G.. The global phosphorus cycle: Past, present, and future. *Elements*, 4(2): 89-95.

684 Fletcher T.D., Shuster W., Hunt W.F., Ashley R., Butler D., Arther S., Trowsdale S., Barraud S., Semadeni-Davies A.,  
685 Bertrand-Krajewski J.L., Mikkelsen P.S., Rivard G., Uhl M., Dagenais D., and Viklander M.. SUDS, LID, BMPs, WSUD

686 and more – The evolution and application of terminology surrounding urban drainage. *Urban Water Journal*, 12(7): 525-542,  
687 2015.

688 Griffioen J.. Extent of immobilisation of phosphate during aeration of nutrient-rich, anoxic groundwater. *Journal of Hydrology*,  
689 320 (3-4): 359-369, 2006.

690 Gunnars A., Blomqvist S., Johansson P., and Andersson C.. Formation of Fe (III) oxyhydroxide colloids in freshwater and  
691 brackish seawater, with incorporation of phosphate and calcium. *Geochim. Cosmochim. Acta*, 66 :745-758, 2002.

692 Genkai-Kato M., Vadeboncoeur, Liboriussen L., and Jeppesen E.. Benthic-planktonic coupling, regime shifts, and whole-lake  
693 primary production in shallow lakes. *Ecology*, 93(3): 619-631, 2012.

694 Hartwig E.O.. Factors affecting respiration and photosynthesis by the benthic community of a subtidal siliceous sediment.  
695 *Marine Biology*, 46: 283-293, 1978.

696 Hansson L.A.. Effects of competitive interactions on the biomass development of planktonic and periphytic algae in lakes.  
697 *Limnology and Oceanography*, 33(1): 121-128, 1988. Henry J.C. and Fisher S.G.. Spatial segregation of periphyton  
698 communities in a desert stream: causes and consequences for N cycling. *Journal of The North American Benthological Society*,  
699 22 (4): 511-527, 2003.

700 He S. and Xu Y.J.. Three decadal inputs of nitrogen and phosphorus from four major coastal rivers to the summer hypoxic  
701 zone of the northern Gulf of Mexico. *Water, Air, and Soil Pollution*, 226: 311, 2015.

702 Jäger C.G. and Borchardt D.. Longitudinal patterns and response lengths of algae in riverine ecosystems: A model analysis  
703 emphasizing benthic-pelagic interactions. *Journal of Theoretical Biology*, 442: 66-78, 2018.

704 Jäger C.G., Hagemann J., and Borchardt D.. Can nutrient pathways and biotic interactions control eutrophication in riverine  
705 ecosystems? Evidence from a model driven mesocosm experiment. *Water Research*, 115: 162-171, 2017.

706 Jones C.E., An K., Blom R.G., Kent J.D., Ivins E.R., and Bekaert D.. Anthropogenic and geologic influences on subsidence  
707 in the vicinity of New Orleans, Louisiana. *JGR Solid Earth*, 121(5): 3867-3887, 2016.

708 Kuenen J.. Anammox bacteria: from discovery to application. *Nature Reviews Microbiology*, 6: 320-326, 2008.

709 Kopáček J., Borovec J., Hejzlar J., Ulrich K., Norton S.A., and Amirbahman A.. Aluminum control of phosphorus sorption by  
710 lake sediments. *Environmental Science & Technology*, 39 (22): 8784-8789, 2005.

711 Kleeberg A., Hupfer M., and Gust G.. Phosphorus entrainment due to resuspension in a lowland river, Spree, NE Germany-A  
712 laboratory microcosm study. *Water, Air, and Soil Pollution*, 183(1-4): 129-142, 2007.

713 Kabenge M., Wang H., and Li F.. Urban eutrophication and its spurring conditions in the Murchison Bay of Lake Victoria.  
714 *Environmental Science and Pollution Research*, 23: 234-241, 2016.

715 Lijklema L.. Nutrient dynamics in shallow lakes: effects of changes in loading and role of sediment-water interactions.  
716 *Hydrobiologia*, 275/276: 335-348, 1994.

717 Li X., Chen M., and Anderson B.C.. Design and performance of a water quality treatment wetland in a public park in Shanghai,  
718 China. *Ecological Engineering*, 35: 18-24, 2009.

719 Le Moal M., Cascuel-Oudoux C., Menesguen A., Souchon Y., Etrillard C., Levain A., Moatar F., Pannard A., Souchu P.,  
720 Lefebvre A., and Pinay G.. Eutrophication: A new wine in an old bottle. *Science of the Total Environment*, 651: 1-11, 2019.

721 Lyvén B., Hassellöv M., Turner D.R., Haraldsson C., and Andersson K.. Competition between iron- and carbon-based colloidal  
722 carries for trace metals in a freshwater assessed using flow field-flow fractionation coupled to ICPMS. *Geochimica et*  
723 *Cosmochimica Acta*, 67(20): 3791-3802, 2003.

724 Li H., Song C.L., Cao X.Y., and Zhou Y.Y.. The phosphorus release pathways and their mechanisms driven by organic carbon  
725 and nitrogen in sediments of eutrophic shallow lakes. *Science of the Total Environment*, 572: 280-288, 2016.

726 Lofts S., Tipping E., and Hamilton-Taylor J.. The Chemical Speciation of Fe(III) in Freshwaters. *Aquatic Geochemistry*, 14(4):  
727 337-358, 2008.

728 Lu H., Wang J., Li J., Shao H., and Wu Y.. Periphytic biofilm: A buffer for phosphorus precipitation and release between  
729 sediments and water. *Chemosphere*, 144: 2058-2064, 2016.

730 Middelburg J.J.. *Marine Carbon Biogeochemistry - A Primer for Earth System Scientists*. Springer Briefs in Earth System  
731 Sciences. Switzerland, 2019.

732 McGlathery K.J., Anderson I.C., and Tyler A.C.. Magnitude and variability of benthic and pelagic metabolism in a temperate  
733 coastal lagoon. *Marine Ecology Progress Series*, 216: 1-15, 2001.

- 734 Mosley L.M., Hunter K.A., and Ducker W.A.. Forces between Colloid Particles in Natural Waters. *Environmental Science &*  
735 *Technology*, 37 (15): 3303-3308, 2003
- 736 Middleburg J.J. and Nieuwenhuize J.. Uptake of dissolved inorganic nitrogen in turbid, tidal estuaries. *Marine Ecology*  
737 *Progress Series*, 192: 79-88, 2000.
- 738 Miller M.P., Tesoriero A.J., Capel P.D., Pellerin B.A., Hyer K.E., and Burns D.A.. Quantifying watershed-scale groundwater  
739 loading and instream fate of nitrate using high-frequency water quality data. *Water Resources Research*, 52: 330-347, 2016.
- 740 Mulder A., van de Graaf A.A., Robertson L.A., and Kuenen J.G.. Anaerobic ammonium oxidation discovered in a denitrifying  
741 fluidized bed reactor. *FEMS Microbiology Ecology*, 1(16): 177-184, 1995.
- 742 Nyenje P.M., Foppen J.W., Uhlenbrook S., Kulabako R., and Muwanga A.. Eutrophication and nutrient release in urban areas  
743 of sub-Saharan Africa-A review. *Science of the Total Environment*, 408: 447-455, 2010.
- 744 Neal, C., Reynolds, B., Norris, D., Kirchner, J. W., Neal, M., Rowland, P., Wickham H., Harman S., Armstrong L., Sleep D.,  
745 Lawlor, A., Woods C., Williams B., Fry M., Newton G., Wright D.. Three decades of water quality measurements from the  
746 Upper Severn experimental catchments at Plynlimon, Wales: an openly accessible data resource for research, modelling,  
747 environmental management and education. *Hydrological Processes*, 25(24), 3818-3830, 2011.
- 748 Nizzoli D., Welsh D.T., and Viaroli P.. Denitrification and benthic metabolism in lowland pit lakes: The role of trophic  
749 conditions. *Science of the Total Environment*, 703: 134804, 2020.
- 750 Nahar, M.S., Zhang, J., Ueda, A. et al. Investigation of severe water problem in urban areas of a developing country: the case  
751 of Dhaka, Bangladesh. *Environmental Geochemistry and Health*, 36: 1079-1094, 2014.
- 752 Painter H.A.. A review of literature on inorganic nitrogen metabolism in microorganisms. *Water Research*, 4: 393-450, 1970.
- 753 Pasterank A., Hillebrand H., and Flöder S.. Competition between benthic and pelagic microalgae for phosphorus and light-  
754 long-term experiments using artificial substrates. *Aquatic Sciences*, 71: 238-249, 2009.
- 755 Putt A.E., MacIsaac E.A., Herunter H.E., Cooper A.B., and Selbie D.T.. Eutrophication forcings on a peri-urban lake  
756 ecosystem: Context for integrated watershed to airshed management. *PLoS ONE*, 4(7): e0219241, 2019.
- 757 Paerl H.W., Scott J.T., McCarthy M.J., Newell S.E., Gardner W.S., Havens K.E., Hoffman D.K., Wilhelm S.W., and  
758 Wurtsbaugh W.A. It Takes Two to Tango: When and Where Dual Nutrient (N & P) Reductions Are Needed to Protect Lakes  
759 and Downstream Ecosystems. *Environmental Science & Technology*, 50: 10805-10813, 2016.
- 760 Rozemeijer J.C. and Broers H.P.. The groundwater contribution to surface water contamination in a region with intensive  
761 agricultural land use (Noord-Brabant, The Netherlands). *Environmental Pollution*. 148(3): 695-706, 2007.
- 762 Rozemeijer J.C., van der Velde Y., van Geer F.C., Bierkens M.F.P., and Broers H.P.. Direct measurements of the tile drain  
763 and groundwater flow route contributions to surface water contamination: From field-scale concentration patterns in  
764 groundwater to catchment-scale surface water quality. *Environmental Pollution*, 158: 3571-3579, 2010a.
- 765 Rozemeijer J.C., van der Velde Y., van Geer F.C., de Rooij G.H., Torfs P.J.J.F. and Broers H.P.. Improving load estimates for  
766 NO<sub>3</sub> and P in surface water by characterizing the concentration response to rainfall events. *Environmental Science &*  
767 *Technology*, 44 (16): 6305-6312, 2010b.
- 768 Rode M., Wade A.J., Cohen M.J., Hensley R.T., Michael J.B., Kirchner J.W., Arhonditsis G.B., Jordan P., Kronvang B.,  
769 Halliday S.J., Skeffington R., Rozemeijer J., Aubert A.H., Rinke K., and Jomaa S.. Sensors in the stream: the high-frequency  
770 wave of the present. *Environmental Science & Technology*, 50: 10297-10307, 2016.
- 771 Scheffer, M.. *Ecology of shallow lakes*, 1st edition. London: Chapman & Hall, 1998.
- 772 Stahl M.O.. Groundwater pumping is a significant unrecognized contributor to global anthropogenic element cycles.  
773 *Groundwater*. 57(3) : 455-464, 2019.
- 774 Spears B.M., Carvalho L., Perkins R., Kirika A., and Paterson D.M.. Sediment phosphorus cycling in a large shallow lake:  
775 spatio-temporal variation in phosphorus pools and release. *Hydrobiologia*, 584: 37-48, 2007.
- 776 Smolders A.J.P., Lamers L.P.M., Lucassen E.C.H.E.T., Van Der Velde G., and Roelofs J.G.M.. Internal eutrophication: How  
777 it works and what to do about it—a review. *Chemistry and Ecology*, 22(2): 93-111, 2006.
- 778 Strayer D.L., Pace M.L., Caraco N.F., Cole J.J., and Findlay S.E.G.. Hydrology and grazing jointly control a large-river food  
779 web. *Ecology*, 89(1): 12-18, 2008.
- 780 Thamdrup B. and Dalsgaard T.. Production of N<sub>2</sub> through anaerobic ammonium oxidation coupled to nitrate reduction in  
781 marine sediments. *Applied and Environmental Microbiology*, 68(3): 1312-1318, 2002.

782 Toor G.S., Occhipinti M.L., Yang Y.Y., Majcherek T., Haver D., and Oki L.. Managing urban runoff in residential  
783 neighbourhoods: Nitrogen and phosphorus in lawn irrigation driven runoff. *PLoS ONE*, 12(6): e0179151, 2017.

784 Van der Grift, B., Broers, H.P., Berendrecht, W., Rozemeijer, J., Osté, L., and Griffioen, J.. High-frequency monitoring reveals  
785 nutrient sources and transport processes in an agriculture-dominated lowland water system. *Hydrology and Earth System  
786 Sciences*, 20(5): 1851-1868, 2016.

787 Van Geer F.C., Kronvang B., and Broers H.P.. High-resolution monitoring of nutrients in groundwater and surface waters:  
788 process understanding, quantification of loads and concentrations, and management applications. *Hydrology and Earth System  
789 Sciences*, 20: 3619-3629, 2016.

790 Van der Grift B., Osté L., Schot P., Kratz A., van Popta E., Wassen M., and Griffioen J.. Forms of phosphorus in suspended  
791 particulate matter in agriculture-dominated lowland catchments: Iron as phosphorus carrier. *Science of The Total Environment*,  
792 631-632: 115-129, 2018.

793 Van der Velde Y., Rozemeijer J.C., de Rooij G.H., van Geer F.C., Broers H.P.. Field-scale measurements for separation of  
794 catchment discharge into flow route contribution. *Vadose Zone Journal*, 9(1): 25-35, 2010.

795 Van der Grift B., Rozemeijer J.C., Griffioen J., and van der Velde Y.. Iron oxidation kinetics and phosphate immobilization  
796 along the flow-path from groundwater into surface water. *Hydrology and Earth System Sciences*, 18: 4687-4702, 2014.

797 Wilczak A., Jacangelo, J.G., Marcinko J.P., Odell L.H., and Kirmeyer G.J.. Occurrence of nitrification in chloraminated  
798 distribution systems. *Journal AWWA*, 88(7): 74-85, 1996.

799 Wang T., Liu G., Gao L., Zhu L., Fu Q., and Li D.. Biological and Nutrient Responses to a Typhoon in the Yangtze Estuary  
800 and the Adjacent Sea. *Journal of Coastal Research*, 32(2): 323-332, 2016.

801 Walsh C.J., Roy J.W., Feminella J.W., Cottingham P.D., Groffman P.M., and Morgan II R.P.. The urban stream syndrome:  
802 current knowledge and the search for a cure. *Journal of The North American Benthological Society*, 24(3): 706-732, 2005.

803 Wriedt, G., Spindler J., Neef T., Meißner R., and Rode M.. Groundwater dynamics and channel activity as major controls of  
804 in-stream nitrate concentrations in a lowland catchment system? *Journal of Hydrology*, 343: 154–168, 2007.

805 Yu L., Rozemeijer J.C., van Breukelen B.M., Ouboter M., van der Vlugt C., and Broers H.P.. Groundwater impacts on surface  
806 water quality and nutrient loads in lowland polder catchments: monitoring the greater Amsterdam area. *Hydrology and Earth  
807 System Sciences*, 22:487-508, 2018.

808 Yu L., Rozemeijer J.C., van der Velde Y., van Breukelen B.M., Ouboter M., and Broers H.P.. Urban hydrogeology: Transport  
809 routes and mixing of water and solutes in a groundwater influenced urban lowland catchment. *Science of the Total  
810 Environment*, 678: 288-300, 2019.

811 Yang Y.Y. and Toor G.S.. Stormwater runoff driven phosphorus transport in an urban residential catchment: Implications for  
812 protecting water quality in urban watersheds. *Scientific Reports*, 8: 11681, 2018. doi: 10.1038/s41598-018-29857-x

813 Zhu W.X., Dillard N.D., and Grimm N.B.. Urban nitrogen biogeochemistry: status and processes in green retention basins.  
814 *Biogeochemistry*, 71: 177-196, 2004.

815 Zhang W., Jin X., Meng X., Tang W., and Shan B.. Phosphorus transformations at the sediment-water interface in shallow  
816 freshwater ecosystems caused by decomposition of plant debris. *Chemosphere*, 201: 328-334, 2018.

817 Zhang X. and Mei X.. Effects of benthic algae on release of soluble reactive phosphorus from sediments: a radioisotope tracing  
818 study. *Water Science and Engineering*, 8(2): 127-131, 2015.

819 Zhou L., Wang S., Zou Y., Xia C., and Zhu G.. Species, abundance and function of ammonia-oxidizing Archaea in inland  
820 waters across China. *Scientific Reports*, 5: 15969, 2015.